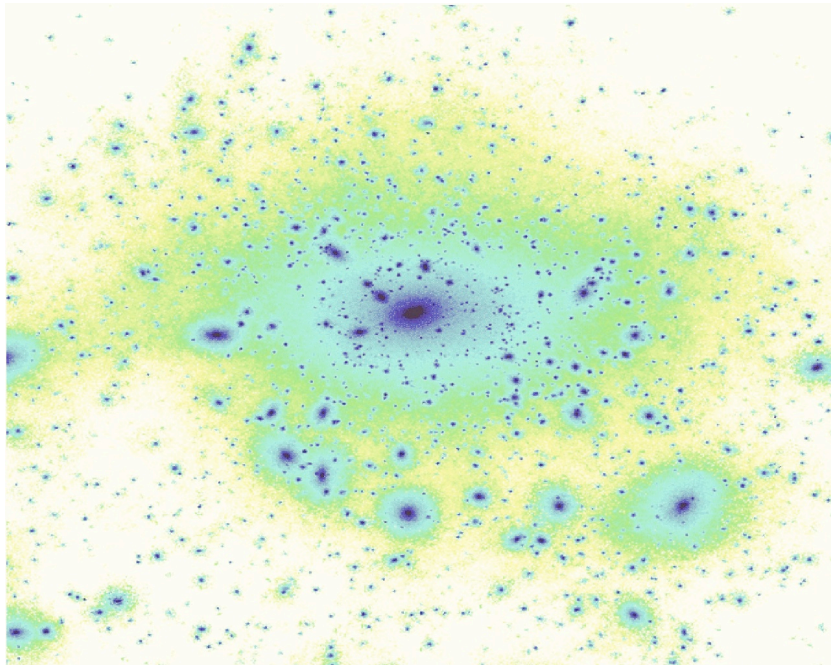


Master's thesis:
On the investigation of dark matter haloes



Teddy Frederiksen,
Dark Cosmology Centre

May 1, 2009

Abstract

In this thesis I will show that it is possible to 1) derive all the physical properties of the gas in clusters of galaxies from the dark matter distribution alone, and 2) that it is possible to use this to determine the dark matter density profile from the surface brightness alone. When the dark matter density profile is known, then other radial profiles of the gas properties, such as temperature or density, can be computed and compared to observations to check if the result is consistent with the assumptions. Besides assuming the validity of the Jeans equation and hydrostatic equilibrium we also assume that there is a linear relation between the density slope and anisotropy ($\gamma \sim \beta$ relation) and a constant relation between the dispersions of the dark matter and the gas (the dark matter temperature relation) which both have been confirmed through numerical simulations.

Acknowledgments

I would like to thank all the people that have helped me during my work on this thesis. First of all I would like to thank my supervisor Steen H. Hansen for giving me the opportunity for doing what turned out to be an exciting project. I would also like to thank Ole Høst for the many discussions and help he has offered during this thesis. Finally I would like to thank Signe Riemer-Sørensen for kindly letting me use her data and all the other people that have helped me during this thesis.

Front picture:

A galaxy sized simulation from Lucio Mayer & Stelios Kazantzidis.

Contents

1	Introduction	4
1.1	History	4
1.2	Cosmology Today	6
1.3	The concordance model(s)	8
2	The basics	11
2.1	Hydrostatic Equilibrium	11
2.2	Observations	15
2.3	Phase-space and the Jeans Equation	16
2.4	Density models	19
3	Kappa	22
3.1	The Hansen-Moore relations	23
3.2	DM temperature	23
3.3	The closed set of equations	25
3.4	A prediction	29
4	Clusters of Galaxies	31
4.1	Case Study: Abell 1689	31
4.2	Results	35
5	Summary	39
5.1	Conclusion	39
5.2	Outlook	40
A	Equations	42
A.1	The gas equation	42
A.2	Surface brightness	44

A.3	The MeKaL model	45
A.4	IDL-implementation	48
A.5	Numerical integration	51
B	Article	53
C	Source Code	63
C.1	kappa1.pro	63
C.2	intloglog.pro	71
C.3	intloglog2.pro	72
C.4	dydx.pro	73
C.5	dlnydlnx.pro	74

Chapter 1

Introduction

Throughout history mankind has looked up to the heavens and tried to answer the question: "What is out there?" This question is still one of the most central questions for any astronomer and much has been learned since the time of the first Greek astronomers. We have among other things discovered the existence of dark matter in the Universe.

In this thesis I will primarily focus on how to determine properties of the dark matter in clusters of galaxies. Galaxy clusters are the biggest gravitationally bound systems in the Universe, but still relatively simple as they primarily only contain gas and dark matter, whereas the stellar component is negligible.

1.1 History

The history of astronomy is almost as old as the history of mankind itself. Every culture from which we have written accounts in some way or another have tried to make sense of the heavens. Among the oldest cultures from which we have written accounts are the Egyptians and the Mesopotamians, and whereas most astronomy of that time would be classified as mythology today, the old Babylonians¹ started a custom that would become the foundation of science: They founded their ideas on logic and what they could observe. This tradition was carried on by the early Greeks who are the founders of modern day astronomy.

¹Babylon was one of the main cities in Mesopotamia

Hipparchus was one of the early Greek astronomers and he invented the magnitude scale of the stars that (with modifications) is still used today. He would call the brightest stars in the night sky "stars of the first magnitude" and the faintest stars that are visible with the naked eye "stars of the sixth magnitude". Today we have flux measurements of the stars that Hipparchus looked at and we can therefore find an empirical relation between the flux and the magnitude of a star. Therefore the modern definition is,

$$M = -2.5 \log \left(\frac{F}{F_0} \right), \quad (1.1)$$

where F_0 is a reference flux that defines the zero-magnitude. The magnitude scale is a logarithmic scale where a difference of 2.5 magnitudes equals a factor of 10 in flux. It is also worth noting that the scale is reversed in the sense that, faint stars have large positive magnitudes and bright stars have low even negative magnitudes. The Greeks not only gave us the magnitude system but also one of the first rational models of the Universe. They believed in the perfection of geometry and that this (divine) geometry also governed the heavens. This led them to believe that the Universe was made up of crystal spheres whereupon the planets revolved, but as the observations of the movements of the Sun, Moon and planets got more extensive they had to modify their model of the Universe. The Greeks believed that the Earth was the center of the Universe and that the Sun, Moon and planets revolved around the Earth in perfect circular orbits. This turned out not to predict the planets' retrograde movement correctly, so they tried to explain this by introducing epicycles, which means that the planets had to move in a small circle as they orbits the Earth. This world model is called Ptolemaic after the Greek/Roman astronomer Ptolemy. All the world views that put the Earth at the center of the Universe are called geocentric.

By the medieval period an astronomer named Galileo Galilei had gotten the idea to construct a telescope to aid him in his investigation of the heavens. He constructed his first telescope after hearing of a practical set of theater binoculars invented in the Netherlands. With the aid of a telescope Galileo found that Venus is not orbiting the Earth, by studying the faces of Venus. He also found the four inner Moons of Jupiter (called the Galilean Moons in his honor) and thereby proved that not everything revolves around the Earth. This discovery lead to the development of other world models where the Sun was in the center, the so called heliocentric world model. There were

different models with a varying number of planets orbiting either the Sun or the Earth.

The next evidence against the Greek model came from the Danish astronomer Tycho Brahe who around the time of Galileo was a very productive observer. He made countless measurements of the night sky. In 1572 he observed a new star in the constellation of Cassiopeia. It was explained as being an object in the atmosphere, but Tycho showed that it had to be situated beyond the Moon and thereby proved that the heavens are not unchanging and eternally the same. In 1577 Tycho observed a comet that he could show had passed through the crystal spheres that the Greeks had postulated existed.

Although Tycho did not believe in a heliocentric Universe his student Johannes Kepler did. Kepler used Tycho's observations of the planets to derive his three laws of planetary motion. These laws broke with one of the last characteristics of the Greek world model: The orbits of the planets are not circular but elliptical. With these laws Kepler could explain the motion of the planets much more accurately and without the use of epicycles. It would be almost a century before Sir Isaac Newton formulated his law of gravity and the laws of Kepler could be explained from a more fundamental theory. Newton's law of gravity also made an impact on the world view, because now the heavens were governed by the same laws that applied on the Earth.

As telescopes got better astronomers began to observe the annual parallax of the nearest stars which enabled them to calculate their distances by simple geometry. These observations put a new minimum size on the Universe. Newton even argued that since gravity is an attractive force and the fact that all matter is not concentrated in one point has to imply that the Universe is infinite.²

1.2 Cosmology Today

The next major change came in 1905 to 1915 when Albert Einstein published his special and general relativity theories. Einstein reintroduced the idea that the Universe was governed by geometry, not in three dimensions but four. Space-time describes the Universe in four dimensions, treating time as a fourth "space" dimension and Einstein general relativity theory explains

²Newton did not take into account that the Universe might have a finite age.

how mass³ curves space-time. In space-time gravity is not a force but a geometric property of space itself. This means that all objects have to follow the shortest path⁴ in space-time like marbles on a rubber sheet. So if there is a massive object in the vicinity the shortest path can become a closed orbit around the massive object. Even light, although massless and thereby unaffected by gravity in Newton's description, has to follow the shortest path which means it can be deflected by heavy objects. This was proven during a solar eclipse where a small deflection of a star near the solar disc was observed, thereby confirming general relativity.

General relativity is the framework of modern cosmology and in general relativity the Universe can have three kinds of morphologies or shapes: Open, flat or closed. An open Universe means that the Universe is infinite and if we draw big triangles it would be like drawing triangles on a saddle, that is, the sum of the angles is less than 180° . Another interpretation would be that two rays of light that are perfectly parallel would in time get further and further apart from each other. The opposite is true for a closed Universe: Parallel rays eventually cross and big triangles have a sum of angles larger than 180° , like the triangles on the surface of a sphere.

Where Einstein made it possible for us to understand the nature of the Universe through space-time it was Edwin Hubble who brought the next piece of evidence that would change our knowledge of the Universe. He showed that the further away an object is, the faster it travels away from us, like if we were sitting in the middle of an explosion. This spawned the Big Bang theory which states that the Universe has a finite age. We know today that the age of the Universe is approximately 13.7 billion years old.

Another piece of our current understanding of the Universe came in 1964 when the two astronomers Arno Penzias and Robert Wilson discovered that there was a constant radio signal from any direction in the sky. This was named the Cosmic Microwave Background (or CMB for short), and has the spectrum of a perfect blackbody with a temperature of $2.7K$. Later observations of the CMB has shown minute fluctuations in the temperature of the order of $\delta T/T \sim 10^{-5}$.

The last few decades has revealed to us that not only are we⁵ in the center of a huge "explosion", but also that the major part of our Universe consists

³Mass and energy are two manifestations of the same thing

⁴The technical term for shortest path is "geodesic"

⁵Actually every point in space is "at the center" of the explosion.

of "dark" components: Dark matter and dark energy.

Dark matter was discovered by looking the velocity dispersion in galaxy clusters and at rotation curves of galaxies. Measurements showed that the galaxies and stars were moving faster than they should be able to, this implied that there has to be extra matter present to keep them from flying apart. The other "dark" component is dark energy which acts as a force against gravity on large scales. The first candidate for explaining this was the cosmological constant that Einstein introduced in his general relativity. This constant can be interpreted as a non-zero vacuum energy that, when gravity becomes weak enough over long distances, takes over and exerts force on the Universe which leads to accelerated expansion. This is what supernova observations have showed. Our Universe is not only expanding it is also accelerating its expansion.

1.3 The concordance model(s)

There are many theories that describe different aspects of the Universe on a cosmological scale, some theories explain the early Universe, some explain the formation of structures in the Universe. In this section I will go through the theories that is believed to best describe our current knowledge of the Universe. These theories are: Inflation, big bang nucleosynthesis, and lambda cold dark matter, among others. I will refer to this group of theories as the concordance models of the Universe.

The first theory is inflation-theory. Inflation is an early epoch right after the Big Bang where the Universe grew approximately $e^{60} \sim 10^{26}$ times in size. This epoch explains why the Universe is so close to being perfectly flat and how the seed of large scale structures formed from quantum fluctuations. These quantum fluctuations can also be seen in the CMB as small temperature fluctuations. Big Bang Nucleosynthesis (BBN for short) describes how the elements in the Universe were produced from the radiation in the young hot Universe and it precisely gives the abundances of hydrogen, helium and trace amounts of heavier elements.

Maybe the most important member of the concordance models in the field of dark matter is the Lambda Cold Dark Matter (or Λ CDM) model. Within the framework of general relativity this model can give a quantitative description of the Universe at the present time. As described above observations have shown that the Universe contains a component that acts

against gravity on large scale and the cosmological constant, (denoted Λ ,) is a force that does that, hence the Λ in Λ CDM.

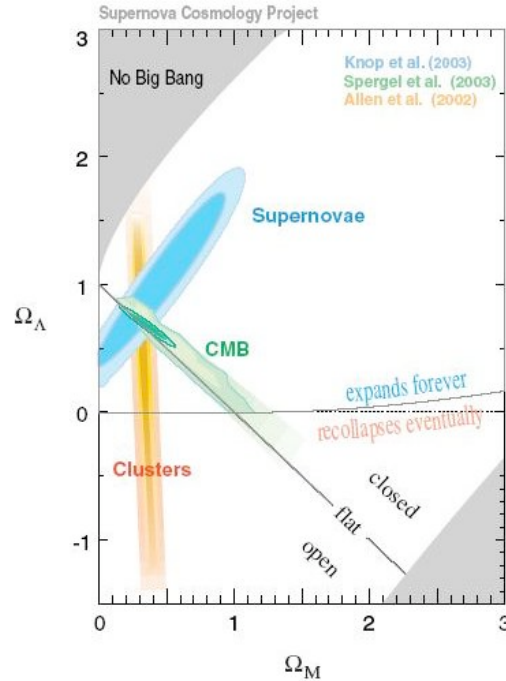


Figure 1.1: Observational constraints on Ω_Λ and Ω_m from the CMB, Supernova standard candles and the matter in clusters of galaxies (see [17]). On the x-axis the amount of matter in the Universe, on the y-axis the amount of cosmological constant (dark energy). Best fit point: $\Omega_m \approx 0.27$, $\Omega_\Lambda \approx 0.73$

Λ CDM characterize the Universe by the components it contains and the amount of them. These components are: radiation, baryons, dark matter, a cosmological constant (or other types of dark energy) and even curvature if a non-flat Universe is considered. The amount of one component is calculated as the energy density of the component compared to a critical energy density⁶, which is denoted Ω_r , Ω_b , Ω_{dm} , Ω_Λ , and Ω_k respectively for the components mentioned above. Observations primarily from the CMB have shown that the present day values of Ω_r and Ω_k are very small, that is, we live in a flat

⁶The critical energy density is the density that is required to keep the Universe (space-time) flat.

Universe with only negligible amounts of radiation energy density today. It is customary to combine Ω_{dm} and Ω_b to a total matter component Ω_m where the dark matter component is the dominant of the two. This means that our Universe can essentially be expressed by two parameters: Ω_m and Ω_Λ . Astronomers today try to determine the values of Ω_m and Ω_Λ with better precision, and the values that best fit the data are approximately $\Omega_m \approx 0.27$ and $\Omega_\Lambda \approx 0.73$ (see figure 1.1).

The Λ CDM model has taught us how structure formation takes place as small over-densities in the young Universe gathers mass. The dark matter clusters together earlier than the baryonic component because dark matter does not exert a repulsive pressure to resist the self-gravity of the over-densities. So by the time the baryons collapse the dark matter has already created a considerable potential well, that the baryons fall into. The dark matter is thus not only the dominant gravitational component but also the dominant factor in the determining the distribution of matter. That is why it is a good approximation only to consider the dark matter when we want to understand the overall structure of the Universe.

We divide the Universe in different domains depending on what scale we are looking at. The term galaxy scale is used when we are looking at an individual galaxy. The term cluster scale is used when we look at entire clusters of galaxies and last the term cosmological scale is used for scales much larger than the biggest galaxy clusters. For each step we go up or down in scale we have to use different kinds of physics: On cosmological scale we need only to know the dark matter distribution and the expansion of the Universe, as described above. On cluster scale (inside a cluster halo) we do not need to take the expansion of the Universe or the individual stars into account, but here gas physics becomes important. Similarly on galaxy scales some physics become unimportant and other physics has to be taken into account, like radiation of gas and star formation.

Chapter 2

The basics

In this section I will introduce all the mathematics and observational concepts that are needed to understand the physics and the observations involved. For that we need some basic definitions of what a cluster is made of.

Clusters of galaxies consist of three constituents: Dark matter, gas, and stars (in galaxies). The most important constituent is dark matter because it is dominating the gravitational potential, the second most dominant constituent is the gas, whereas the stellar component only has negligible mass. The gas component is called the Intra-Cluster Medium (or ICM for short), and consists mostly of primordial gas from the Big Bang. It is mostly hydrogen, eventually enriched with the gas ejected from the galaxies. The galaxies might have a higher metallicity due to metal enrichment from supernova explosions. The gas is very hot and therefore fully ionized (that is, plasma)¹. The gas is also very dilute with a number density of the order 10^{-3} atoms per cubic cm which gives a mean free path of the order 10^{16} meters (one third parsec). So in the absence of magnetic fields the ICM can very well be approximated by an ideal gas. From the gas we observe thermal bremsstrahlung which we use to infer the properties of the gas.

2.1 Hydrostatic Equilibrium

In this section I will give an introduction to fluid mechanics. I will just go through what is required for the treatment of the ICM. For a more in-depth treatment of fluid mechanics see [18].

¹The proper term would be "plasma" but the term "gas" is widely used in the literature.

We will start by considering a small volume of fluid, dV , a so-called fluid-element. The force acting on a surface-element $d\vec{A} = \vec{n} dA$ is,

$$-p d\vec{A} = -p \vec{n} dA, \quad (2.1)$$

where \vec{n} is a unit vector pointing out of the fluid element whereas the force is pointing inwards, hence the sign. If we integrate the force over the surface of the fluid-element we get an integral that via Green's theorem can be turned into,

$$-\oint p d\vec{A} = -\int \vec{\nabla} p dV, \quad (2.2)$$

where $\vec{\nabla}$ is the *del* operator (vector differential operator), and $-\vec{\nabla} p$ has the unit of force per unit volume. This force per unit volume can be inserted into the fluid equivalent of Newton's second law,

$$\rho \frac{d\vec{v}}{dt} = -\vec{\nabla} p, \quad (2.3)$$

where ρ is the density, and $\frac{d\vec{v}}{dt}$ the acceleration. $\frac{d\vec{v}}{dt}$ is, however, not a simple vector because the fluid-element is not a rigid or point like element. Therefore, we have to take the variation of all the coordinates into account:

$$d\vec{v} = dt \frac{\partial \vec{v}}{\partial t} + dx \frac{\partial \vec{v}}{\partial x} + dy \frac{\partial \vec{v}}{\partial y} + dz \frac{\partial \vec{v}}{\partial z}. \quad (2.4)$$

We divide by dt and substitute $\frac{dx_i}{dt} = v_i$,

$$\frac{d\vec{v}}{dt} = \frac{\partial \vec{v}}{\partial t} + v_x \frac{\partial \vec{v}}{\partial x} + v_y \frac{\partial \vec{v}}{\partial y} + v_z \frac{\partial \vec{v}}{\partial z}. \quad (2.5)$$

The last three terms look like a vector dot product between the velocity and the $\vec{\nabla}$ operator. This can then be simplified to,

$$\frac{d\vec{v}}{dt} = \frac{\partial \vec{v}}{\partial t} + (\vec{v} \cdot \vec{\nabla}) \vec{v}. \quad (2.6)$$

The same consideration has to be made for every time derivative on a fluid element not just when we want to differentiate \vec{v} , this is why it is customary to define the operator,

$$\frac{d}{dt} = \frac{\partial}{\partial t} + (\vec{v} \cdot \vec{\nabla}), \quad (2.7)$$

which is called the material or substantial derivative. This derivative also appears in the conservation-of-mass law,

$$\frac{d\rho}{dt} = \frac{\partial\rho}{\partial t} + (\vec{v} \cdot \vec{\nabla})\rho = 0. \quad (2.8)$$

The first derivative can be interpreted as the derivative in the comoving frame, that is, the density has to be constant in the comoving frame, where as the other terms say that the change in density has to be balanced by what flows in or out of the fluid-element.

We want to use the definition of differentiation on a fluid-element to restate equation (2.3) as,

$$\rho \left(\frac{\partial\vec{v}}{\partial t} + (\vec{v} \cdot \vec{\nabla})\vec{v} \right) = -\vec{\nabla}p + \vec{f}_{ext}, \quad (2.9)$$

where \vec{f}_{ext} are the external forces that act on the fluid element. Equation (2.9) is called the Euler equation² after Leonhard Euler who derived it for the first time. In this treatment I will only consider one external force, gravity,

$$\vec{f}_{ext} = \rho\vec{g} = -\rho\frac{GM(r)}{r^2}\vec{r}, \quad (2.10)$$

where $M(r)$ is the mass interior to the radius r from the center of a spherical potential and \vec{r} is the radial unit vector. We insert this into equation (2.9),

$$\frac{\partial\vec{v}}{\partial t} + (\vec{v} \cdot \vec{\nabla})\vec{v} = -\frac{1}{\rho}\vec{\nabla}p - \frac{GM(r)}{r^2}\vec{r}. \quad (2.11)$$

This equation will serve as one of our main equations. It will be rewritten in many forms, but it serves as the theoretical background for many of the properties we derive for the ICM.

We now want to rewrite this equation to give us the mass. We make the simplification that our mass is spherically distributed and at rest. We thereby get rid of the left hand side (the velocity terms) of equation (2.11) and $\vec{\nabla}$ becomes $\frac{d}{dr}$ because there can only be a gradient in this direction due to spherical symmetry:³

$$\frac{1}{\rho} \frac{dp}{dr} = -\frac{GM(r)}{r^2}. \quad (2.12)$$

²The Euler equations (plural) are actually a set of equations, but when referred to in the singular this equation is implied

³Equation (2.12) is called hydrostatic equilibrium. It states that pressure and gravity has to be balanced out.

As described in the introduction to this section we know that the ICM can be described very well by an ideal gas, and for ideal gasses the pressure is given by

$$p = \frac{kTN}{V} = \frac{kT\rho}{m} \quad (2.13)$$

where k is Boltzmann's constant and N is the number of particles with a mass m , in volume V . It is customary to write the particle mass as a mean molecular weight μ times the proton mass $m = \mu m_p$.

We insert equation (2.13) into equation (2.12) and get

$$\frac{1}{\rho} \frac{d}{dr} \left(\frac{kT\rho}{\mu m_p} \right) = \frac{k}{\mu m_p \rho} \frac{d(T\rho)}{dr} = -\frac{GM(r)}{r^2}. \quad (2.14)$$

Now we rewrite this by using the definition of the logarithmic derivative $\frac{d \ln y}{d \ln x} = \frac{x}{y} \frac{dy}{dx}$ to get

$$\frac{kT}{\mu m_p} \frac{d \ln(T\rho)}{d \ln r} = -\frac{GM(r)}{r}. \quad (2.15)$$

The logarithmic derivative makes it possible to expand a product to a sum like the ordinary logarithm. Now we isolate M and expand the product to obtain,

$$M(r) = -\frac{kT}{G \mu m_p} r \left[\frac{d \ln T}{d \ln r} + \frac{d \ln \rho}{d \ln r} \right]. \quad (2.16)$$

This is the mass equation derived from the hydrostatic equilibrium, in astrophysical context this equation is often just called hydrostatic equilibrium. It is also one of the main ways of weighing a galaxy cluster since the total matter $M(r)$ is given from the gas properties alone (see e.g. [29]), as both temperature and density of the gas can be derived from X-ray observations. Even if the assumptions are broken by some perturbation of the cluster, this equation just becomes an *estimator* of the mass. The estimate will in general be of the same order as the true mass distribution (see [24]). If we had rewritten equation (2.11) and kept the velocity terms we would had ended up with,

$$M(< r) = -\frac{kT}{G \mu m_p} r \left[\frac{d \ln T}{d \ln r} + \frac{d \ln \rho}{d \ln r} \right] + \frac{r^2 v_r}{G} \frac{dv_r}{dr} - \frac{r v_{rot}^2}{G}, \quad (2.17)$$

where only spherical symmetric velocity terms can enter due to spherical symmetry.⁴

⁴This equation is actually oversimplified as the mass interior to r , $M(< r)$, is also dependent on the angular coordinates in any real scenario involving velocities.

The impact of bulk motion and inclusion of the velocity terms has been treated thoroughly and independently by Kasper Schmidt (see [28]) and Joel Johansson (see [15]).

2.2 Observations

When we want to know something about the ICM we start by taking a spectrum in X-rays. This spectrum will in the general case look like figure 2.1. The form of the spectrum can be characterized by a smooth curve with added

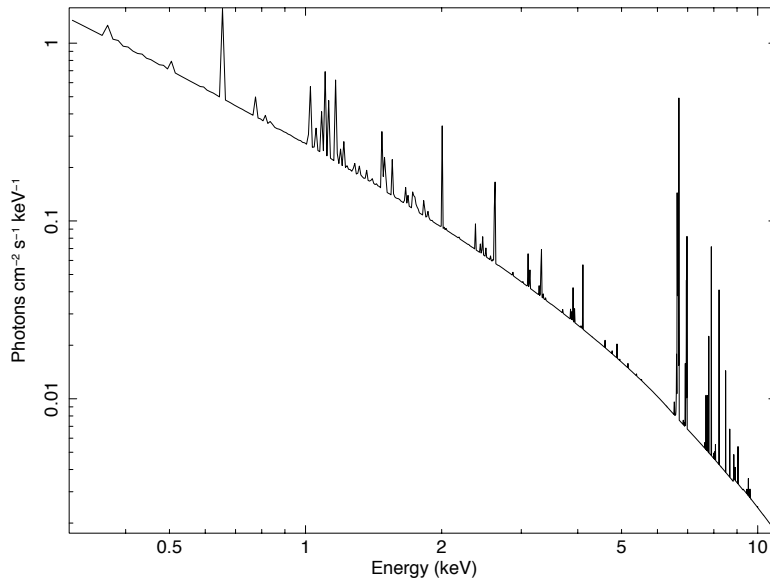


Figure 2.1: A sample X-ray spectrum showing the Intensity as a function of energy. The spectrum can be split up into the emission lines (the spikes) which gives the gas density and the continuum (the smooth curve) which gives the temperature

spikes. The smooth part is called the continuum part and goes like e^{-T} , which can be used to give us the temperature. The spikes are the emission lines from the atoms in the ICM when they reemit a photon. The height of the emission lines gives us the density of the gas. When we then have both the density and the temperature for different radii we can use the mass equation (2.16) to derive the mass distribution and thereby weigh the cluster.

2.3 Phase-space and the Jeans Equation

As dark matter is collisionless and only interacts via gravity, we could in principle solve Newton's equations for all the individual particles. This would, however, be an overwhelming task, instead we take a continuum approach like for the ICM. The formalism of a collisionless continuum is the phase-space (\vec{x}_i, \vec{v}_i) and the distribution function $f(\vec{x}_i, \vec{v}_i, t)$. For a more in-depth treatment on collisionless systems see [1].

Phase-space is the combined space of position and velocity. A particle with position $\vec{x} = (x, y, z)$ and velocity $\vec{v} = (v_x, v_y, v_z)$ would have the coordinate $\vec{w} = (\vec{x}, \vec{v}) = (x, y, z, v_x, v_y, v_z)$ in phase-space. A distribution function, f , gives the probability of finding a particle in a volume $d^6V = d^3x d^3v$ so the probability of finding a particle inside a volume V is,

$$P = \int_V f(\vec{x}, \vec{v}, t) d^3\vec{x} d^3\vec{v}. \quad (2.18)$$

Like the conservation of mass for gasses we need also a conservation law that insures us that our collisionless fluid does not disappear. In collisionless systems this becomes the conservation of probability. They are both equivalent to the conservation of the total number of particles. In index notation this conservation law becomes,

$$\frac{df}{dt} = \frac{\partial f}{\partial t} + \frac{\partial w_i}{\partial t} \frac{\partial f}{\partial w_i} = 0 \quad (\text{sum over } i), \quad (2.19)$$

where $w_i = \{x, y, z, v_x, v_y, v_z\}$. If we rewrite the last term on the left hand side in three dimensional real-space coordinates instead of six dimensional phase-space coordinates and use the Hamiltonian formalism the equation becomes:⁵

$$\frac{df}{dt} = \frac{\partial f}{\partial t} + v_i \frac{\partial f}{\partial x_i} - \frac{\partial \Phi}{\partial x_i} \frac{\partial f}{\partial v_i} = 0 \quad (\text{sum over } i), \quad (2.20)$$

where $x_i = \{x, y, z\}$, $v_i = \{v_x, v_y, v_z\}$ and Φ is the gravitational potential. We have used the fact that the acceleration is given by the gradient of the potential. This is the collisionless Boltzmann equation which is the underlying governing equation for collisionless systems.

⁵The thorough derivation can be seen in [1] p. 276-277.

It is, however, not an easy task to find the distribution function of a particular system, but it turns out that if we take the zeroth and first momentum of equation 2.20, we end up with quantities that can be either directly observed or by other means observationally inferred.

We find the first moment by integrating equation (2.20) over all velocities to get

$$0 = \int \frac{df}{dt} d^3\vec{v} = \frac{\partial}{\partial t} \int f d^3\vec{v} + \frac{\partial}{\partial x_i} \int v_i f d^3\vec{v} - \frac{\partial \Phi}{\partial x_i} \underbrace{\int \frac{\partial f}{\partial v_i} d^3\vec{v}}. \quad (2.21)$$

We define the probability density at x as $\nu(x) = \int f dv$ and the mean velocity at x as $\bar{v}_i(x) = \nu^{-1} \int v_i f dv$. To get rid of the marked integral we use the fact that no particle moves with infinite velocity. Then we can rewrite the equation as,

$$\frac{\partial \nu}{\partial t} + \frac{\partial \nu \bar{v}_i}{\partial x_i} = 0. \quad (2.22)$$

This equation looks like the conservation of mass equation for fluids and can be interpreted in the same way as the particle density is conserved. It is worth noting that the zeroth moment of the Boltzmann equation, which deals with phase-space, gives a "conservation law" in real-space.

Next we look at the first moment of equation (2.20):

$$\int v_j \frac{df}{dt} d^3\vec{v} = 0 \quad (2.23)$$

The same arguments as for the zeroth moments are used together with equation (2.22) to bring this equation into the following form⁶

$$\nu \frac{\partial \bar{v}_j}{\partial t} + \nu \bar{v}_i \frac{\partial \bar{v}_j}{\partial x_i} = - \frac{\partial(\nu \sigma_{ij}^2)}{\partial x_i} - \nu \frac{\partial \Phi}{\partial x_j} \quad (2.24)$$

where $\sigma_{ij}^2 = \overline{v_i v_j} - \bar{v}_i \bar{v}_j$ is the velocity-dispersion tensor. This equation is the collisionless equivalent of the Euler equation (2.9) and is called the Jeans equation,⁷ where $\nu \rightarrow \rho$, $\bar{v}_j \rightarrow \vec{v}$ and $\nu \sigma_{ij}^2 \rightarrow p$. The thing to note here is

⁶The thorough derivation can be seen in [1] p. 348.

⁷The term "Jeans equations" (plural) is the term for all the moments of the collisionless Boltzmann equation, but if it is referred to as "*the* Jeans equation" in the singular then equation (2.24) is implied.

that whereas pressure for fluids is a scalar quantity, its equivalent in collisionless systems is a tensor quantity. This stems from the collisionless nature of equation (2.20), as the pressure in gasses can be described by a single distribution function (given by the temperature), whereas for collisionless systems the transfer of energy and momentum cannot happen by collision, so the distribution function can be different for the different directions.

Like the Euler equation the Jeans equation can be rewritten in a form that directly can give the matter distribution and this form is the most used in the astronomical literature.

We start by rewriting the Jeans equation in spherical coordinates and switch notation:⁸

$$\frac{\partial \rho \sigma_r^2}{\partial r} + 2\beta \frac{\rho \sigma_r^2}{r} = -\rho \frac{GM(< r)}{r^2}, \quad (2.25)$$

where we have substituted $-\frac{\partial \Phi}{\partial r} \rightarrow \frac{GM(< r)}{r^2}$, $\nu \rightarrow \rho$, $\overline{v_r^2} \rightarrow \sigma_r^2$ and introduced the velocity anisotropy as $\beta = 1 - \frac{\sigma_t^2}{\sigma_r^2}$. We now divide by $\frac{\rho \sigma_r^2}{r}$ and solve for M to get,

$$M(r) = -\frac{\sigma_r^2 r}{G} \cdot \left(\frac{d \ln \sigma_r^2}{d \ln r} + \frac{d \ln \rho}{d \ln r} + 2\beta \right). \quad (2.26)$$

This looks almost identical to the mass formula for the ICM with the small difference that the anisotropy parameter enters. This is again because of the collisionless nature of the dark matter.

The original equations with ν and $\overline{v_r^2}$ were derived to be used in star counting observations because stars are essentially point particles and therefore collisionless in the potential of a galaxy. At that time it was still believed that the stars dominated the potential. It was before "the missing mass" problem that lead to the introduction of dark matter (see [32]), but the validity still holds since the stars can be thought of as test-particles to infer the shape of the potential. Figure 2.2 shows such an application of the Jeans equation for the Draco dwarf spheroidal (a dwarf galaxy) that orbits the Milky Way. Draco is clearly visible as a horizontal feature moving at almost 300 *m/s* towards us. From figure 2.2 it is clear that the number of stars (that is ν) and the width (that is σ^2) decreases with radius. This can be put into the Jeans equation and has revealed that Draco dSph contains almost 400 times more dark matter than luminous matter (see e.g. [16]).

⁸See [1] p 350.

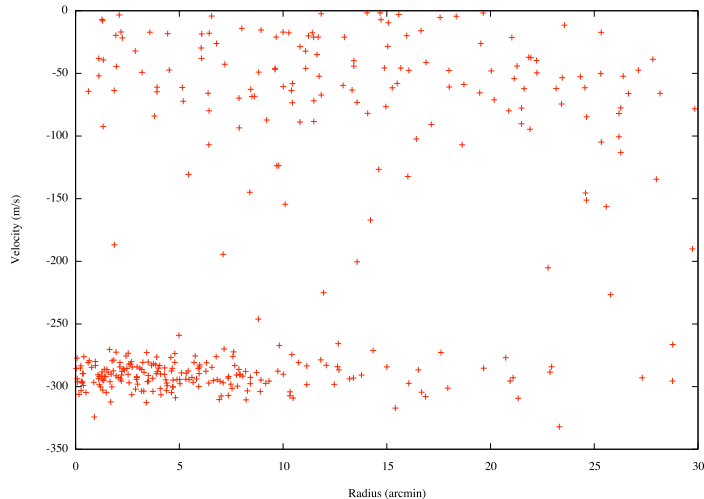


Figure 2.2: Velocity chart for Draco dSph, which is clearly visible at the bottom (see [30]). The x-axis is the radius from the center of Draco dSph, the y-axis is the recession speed (negative means coming towards us). The top is the galactic background stars. Each point is an AGB-star

2.4 Density models

In theoretical treatments in general there is a need to parameterize a given observational quantity with analytical functions, to be able to use the data in the theory. That is done by fitting a proposed function to the observations of e.g. the surface brightness, density, or temperature profile. In the treatment of dark matter the quantity that has received the most attention is the radial density profile.

The most used density model for dark matter is without doubt the NFW model (see [22]) that Navarro, Frenk and White got from investigating numerical simulations. They saw that the density profile of different halos possessed the same features, that is, a universal inner slope that gradually changed to a steeper but equally universal outer slope. They summarized that to a universal density profile of,

$$\rho(r) = \frac{\rho_0}{\frac{r}{r_0} \cdot \left(1 + \frac{r}{r_0}\right)^2}, \quad (2.27)$$

a	b	c	Model
1	3	1	NFW
1	4	1	Hernquist
2	2	-	SIS*
0	2	2	King
0	5	2	Plummer
2	4	1	Jaffe

Table 2.1: List of the different double power law density models. The Singular Isothermal Sphere (SIS) is actually only a single powerlaw but is always used in the same context as the other models.

where ρ_0 and r_0 are scaling quantities for the individual dark matter halo. This is called a double power law because it behaves like a power law with slope -1 for $r \ll r_0$ and a slope of -3 at $r \gg r_0$.

In connection with the NFW profile, the concept of concentration should be introduced. Concentration is observed as a tighter clustering of the mass in heavy clusters, that is, heavy clusters have a bigger part of their mass closer to the center, whereas less heavy clusters have their mass distributed further from the center. There is a relation between the mass of the cluster and the concentration (see e.g. [5]) where more massive clusters have higher concentration and less massive have lower concentration.

Many density models can actually be put in the category of a double power law, by generalizing the power law to

$$\rho(r) = \frac{\rho_0}{\left(\frac{r}{r_0}\right)^a \left(1 + \left(\frac{r}{r_0}\right)^c\right)^{\frac{b-a}{c}}}, \quad (2.28)$$

where $-a$ is the inner slope, $-b$ is the outer slope and c is the strength of the transition between inner and outer (see [13] and [31]). We are able to summarize the double power law models by a , b , and c . A few density models are listed in table 2.1 All the models with an inner slope, a , of zero are called cored and those with an inner slope different from zero are called cusped.

The double power law models are not the only candidates for the density profile on the market. A model that has to be mentioned in the same context as NFW is, the Sersic or Einasto profile. The Sersic profile is a generalization of the de Vaucouleurs profile that is used to fit surface brightness profiles of

elliptical galaxies,

$$I(r) = I(r_e) \exp(-b(x^{1/n} - 1)) , \quad x = \frac{r}{r_e} , \quad (2.29)$$

where an index of $n = 4$ would correspond to the de Vaucouleurs profile. The Estonian astronomer Jaan Einasto suggested that this profile could be used for the radial density profile as well. The big difference is that surface brightness is a quantity in the plane of the sky whereas the density is a quantity in three dimensional space, and the Sersic density profile does not convert into the Sersic surface brightness. The idea of using a rolling slope density profile has turned out to fit well with numerical simulations (see e.g. [23]).

Simulations find that the index $n \sim 1 - 10$ for all reasonable dark matter halos, it even turns out that the index correlates with mass such that small halos like dwarf galaxies have index of $n \sim 6 - 7$ and large galaxy clusters have $n \sim 5$ (see e.g. [20] and [8]). This is because more massive halos are more concentrated than less massive ones.

The final answer to what the universal shape of the dark matter halo should be or even if the shape is a universal quantity is not settled in the scientific community.

Chapter 3

Kappa

From the Jeans equation and hydrostatic equilibrium, introduced in the last chapter, we can find the distribution of matter in a dark matter system if we know either the temperature T and gas density ρ_g , or the density, ρ_{dm} , and velocity dispersion, σ_r^2 , of the dark matter. There are, however, potentially a lot of factors that can bias the results in some form or the other. The first is that we can only infer quantities in the plane of the sky, such as the temperature and density. These quantities have to be deprojected before they can be inserted into the Jeans equation or the hydrostatic equilibrium with,

$$f_{3d}(r) = -\frac{1}{2\pi r} \int_r^\infty \frac{df_{2d}(R)}{dR} \frac{1}{\sqrt{r^2 - R^2}} dR, \quad (3.1)$$

which can be sensitive to small perturbations and uncertainties in the measurements, especially since the integral is taken from infinity and inwards. That means that small uncertainties in the outer region can propagate and accumulate inwards.

That is why I want to turn this around and try to model the dark matter halo, so I can calculate the physical properties directly. In that case the uncertainties don't have to be propagated through the equations. I will in the following treatment try to only make assumptions that are also made in the standard analysis of observational data i.e. spherical symmetry, that hydrostatic equilibrium holds, and that the Jeans equation holds. The two mass equations are remarkably similar and an obvious thing to do is to equate them,

$$M = -\frac{kT}{G \mu m_p} r \left[\frac{d \ln T}{d \ln r} + \frac{d \ln \rho_g}{d \ln r} \right] = -\frac{\sigma_r^2 r}{G} \cdot \left(\frac{d \ln \sigma_r^2}{d \ln r} + \frac{d \ln \rho_{dm}}{d \ln r} + 2\beta \right). \quad (3.2)$$

In this equation there are five variables: T , ρ_g , ρ_{dm} , σ_r^2 , and β . Of these some can be calculated from the others. The dark matter density, ρ_{dm} , can be calculated from the mass given by hydrostatic equilibrium if we assume that the dark matter is the dominant component. The dispersion, σ_r^2 , can also be calculated because when we know M and ρ_{dm} we can solve the Jeans equation for,

$$\sigma_r^2(R) = -\frac{1}{\tilde{\rho}(R)} \int_R^\infty \frac{GM(r) \tilde{\rho}(r)}{r^2} dr, \quad (3.3)$$

where $\tilde{\rho}(r)$ is a function that satisfies the following equation: $\frac{d \ln \tilde{\rho}}{d \ln r} = \frac{d \ln \rho}{d \ln r} + 2\beta$. This still means that we have to know three things about our system: ρ_g , β , and T .

In this treatment we would like the three free parameters to be ρ_{dm} , β , and T because this lets us compute all the quantities from the dark matter density if we can find two connections between dark matter – anisotropy and dark matter – temperature. From numerical simulations such two relations have appeared.

3.1 The Hansen-Moore relations

The first connection that we want to include as an assumption is a proposed relation between the density slope, $\gamma_{dm} = \frac{d \ln \rho_{dm}}{d \ln r}$, and the anisotropy, β , that was first proposed by Hansen and Moore in 2006. This has been investigated further and has been confirmed by various numerical simulations (see [9], [10] and [12]).

The relation is valid in the range $-\gamma \approx 1 - 3$, because in the very central parts of the dark matter simulation where $\gamma \approx -1$, we approach the softening length of the simulation, which introduces numerical noise into the equation. As we go out to the outer parts of the dark matter structure where, $-\gamma \approx 3$, we reach the parts of the structure that is not yet in equilibrium. Analysis of many dark matter simulations have revealed the current best fit to be: $\beta = -0.2(\gamma_{dm} + 0.8)$ with a scatter in β of ± 0.05 .

3.2 DM temperature

To find the second fundamental relation we would like to look at how gas and dark matter interact. Gas interacts with itself as the gas particles collide and

exchange momentum and energy and thereby settle into an equilibrium configuration. This is called thermalization and has the effect that the velocity distribution becomes isotropic, and we can derive a well-defined temperature from the velocity distribution. Dark matter on the other hand is collisionless which means that it cannot thermalize so the velocity distribution for different directions do not have to be equal and hence the total three-dimensional velocity distribution can be anisotropic. That is why β enters in the equations derived from the Jeans equation.

For a particle to stay inside the gravitational potential it needs to have a velocity that is lower than the escape velocity of the potential. If this is the case the particle will stabilize in an orbit corresponding to its energy. That on the other hand implies that when the potential has settled down into equilibrium, the average kinetic energy at a given radius should be of the same order, independent of particle type. This is why the gas dispersion should be of the same order as the average dark matter dispersion,

$$\sigma_{dm}^2 = \frac{1}{3}(\sigma_r^2 + \sigma_\phi^2 + \sigma_\theta^2) = \sigma_r^2(1 - \frac{2}{3}\beta), \quad (3.4)$$

where σ_ϕ^2 and σ_θ^2 are the dispersions along the two tangential directions and σ_r^2 is the velocity dispersion along the radial direction.

All this implies that if the gas does not receive or lose energy through other channels the dark matter makes the gas follow the average velocity distribution of the three directions in the dark matter. We will parameterize this by κ , which is the ratio between the dark matter and the gas dispersions,

$$\kappa = \frac{\sigma_{dm}^2}{\sigma_{gas}^2}. \quad (3.5)$$

For the sake of convenience we can define a dark matter "temperature" although the velocity distribution does not give a well defined temperature in the classical sense. We use the equation that relates temperature and dispersion to define a "temperature" from the average dark matter dispersion,

$$\frac{kT_{dm}}{\mu m_p} = \sigma_{dm}^2 = \sigma_r^2(1 - \frac{2}{3}\beta). \quad (3.6)$$

This makes it possible to write κ in the form,

$$\kappa = \frac{\sigma_{dm}^2}{\sigma_{gas}^2} = \frac{T_{dm}}{T_{gas}}. \quad (3.7)$$

This is also why the molecular weight, μ , in equation (3.6) is the mean molecular weight of the gas and not the dark matter, in order to make κ take the value one. The $\kappa = 1$ relation is called the dark matter temperature relation, and has been confirmed in numerical simulations (see [14]).

If $\kappa > 1$ then heat is removed from the gas, maybe through cooling flows¹ and $\kappa < 1$ implies that heat is added to the gas for example via ram pressure from infall or merger or heating from a central AGN.

Ideas like this are not new. Back in 1986 Craig L. Sarazin stated the same point in his review paper [26]. It was at that time believed that the galaxies were dominating the gravitational potential, so he stated as a prediction that $\sigma_{gas}^2 \sim \sigma_{gal}^2$, as the galaxies can be considered collisionless because the stars do not collide, only the gas gets striped from the galaxies.

3.3 The closed set of equations

Different people have tried different approaches for closing the set of equations. One approach has been to assume the phase-space density $\rho\sigma_r^{-3}$ is a perfect power law and then derive everything else from this (see [6]), but the validity of that assumption has been questioned (see [27]). Alternately one could also start with assuming that the entropy profile has a particular shape and derive the rest from that (see [3]), but there is not a general consensus on the shape of the gas entropy profile or whether there exist a universal shape. In this work we will, however, be working with the two above mentioned assumptions: $\gamma \sim \beta$ and $\kappa = 1$.

With this set of closed equations I will now try to derive all the physical quantities and thereby show that the system is fully determined, given a density profile. We start by combining the DM temperature relation ($\kappa = 1$), hydrostatic equilibrium, and the Jeans equation to get our main equation, the gas equation:

$$\gamma_g = F_\beta \cdot \left[\gamma + 2\beta + \frac{2}{3}\beta \frac{d \ln \sigma_r^2}{d \ln r} - \frac{2}{3} \frac{d\beta}{d \ln r} \right], \quad (3.8)$$

where F_β is shorthand for the fraction $F_\beta = \frac{1}{1-\frac{2}{3}\beta}$ which equals one when β is zero. For the derivation see appendix A.1.

¹The gas is constantly radiating of energy via bremsstrahlung

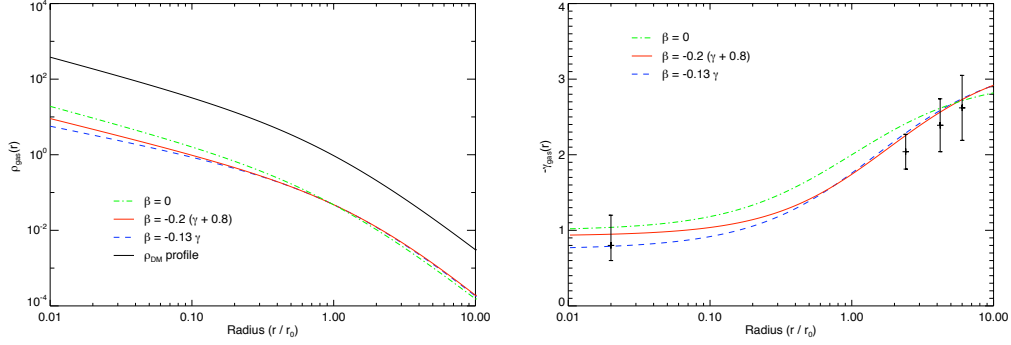


Figure 3.1: Gas density (left) and slope (right) as a function of radius calculated from equation (3.8). The different curves show the effect of varying the anisotropy relation.

This equation gives us the link between the dark matter and gas, because equation (3.8) only contains dark matter (and derived quantities of that) on the right hand side and only the gas shape on the left hand side. This equation in loose terms states: "Dark matter dictates the gas where to be."

In appendix A.4 the precise computation from a given dark matter profile to the gas profile is given, together with the numerical methods used. The in-depth treatment of this topic can be read in the article appended in the appendix, which is submitted to *The Astrophysical Journal* for publication, and is currently in the process of peer review.

Here I want to go through some of the results of the calculations. I have assumed that the dark matter is distributed as an NFW profile for illustrative purposes. Figure 3.1 (left) shows the density profile of the gas compared to the dark matter. The upper curve is the dark matter density and the three lower ones are the gas densities derived with the gas equation. There is not much difference between the three gas curves, which means that the gas density is not that sensitive to the shape of the β profile. If we look at the slope of the gas density in figure 3.1 (right) we see a little more detail. The difference becomes a little clearer but overall the three profiles show the same shape. The dark matter slope would coincide with the $\beta = 0$ curve, which means that the gas density profile in general would tend to be more shallow (flat) than the dark matter if anisotropy is present. The data points are taken from [7] and [29] and show the average values of the gas slope to

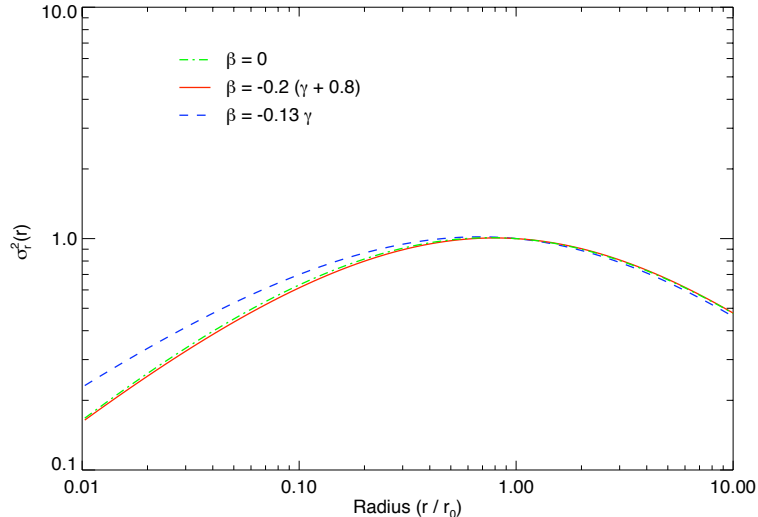


Figure 3.2: The velocity dispersion as a function of radius from equation (3.3), used to calculate the temperature profile with the DM-temperature relation. The different curves show the effect of varying the anisotropy relation.

give an idea of the general shape of the gas slope. The inner data-point is an average inner gas slope of 16 relaxed nearby clusters, whereas the outer data points are the estimates derived from the surface brightness of the outer region of 11 clusters, both data sets are obtained with Chandra.

The dispersion is also easily computed from equation (3.3) and is shown in figure 3.2. Again the overall shapes are similar but this time curve number three ($\beta = -0.13\gamma$) differs towards the center. This is because the anisotropy in the center is larger for that curve ($\beta = 0, 0.04,$ and $0.13,$ respectively for the three curves in the center). If the DM temperature relation holds the temperature profile should follow the dispersion profile. This is in general the case since we usually see a rise in temperature from the center out to a certain radius after which it falls down to the temperature of the ambient surroundings². This case is defined as a *Cool Core* cluster (or CC) whereas if the maximum temperature is in the center it is called a *Non-Cool Core* cluster (or NCC). This can probably be explained by a central AGN injecting energy

²The ambient temperature is 3 K if there are no structures nearby

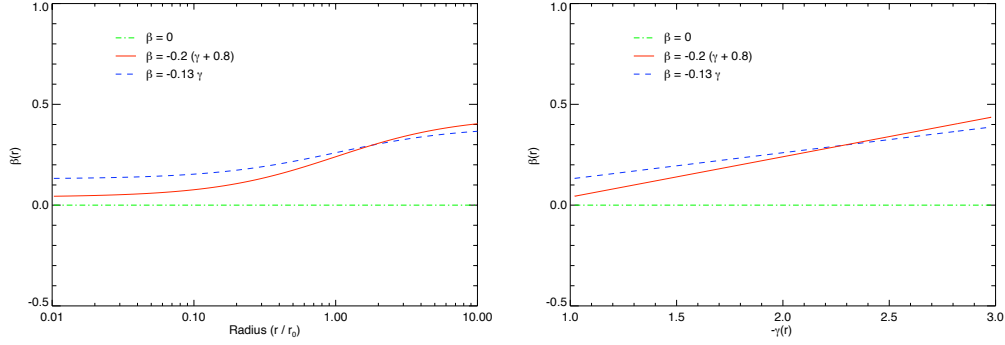


Figure 3.3: The three different beta profiles used in the analysis. Left: β vs radius. Right: β vs γ .

into the gas, which would make κ smaller than unity. Another possibility is that a big cD galaxy is sitting in the center of the cluster and perturbs the cluster which could make κ both larger or smaller than unity.

We have not limited ourselves to only the best fit choice of the $\gamma \sim \beta$ relation, we have chosen three candidates to show the effect of variation of the β profile (see figure 3.3).

The first profile, $\beta = 0$, is a common choice because it makes the Jeans equation and the Hydrostatic Equilibrium look the same and thereby simplifies the equations and the physics involved. We know from the $\gamma \sim \beta$ relation (i.e. numerical simulations) that β is negligible in the center but only there as the velocities further out are radially dominated, with $\beta \approx 0.5$. (see [14])

The second β profile is the current best fit from numerical simulations (see [9]) which shows the small values in the center and the value of approximately one half in the outskirts.

The third profile is an attempt to derive the shape of the $\gamma \sim \beta$ relation analytically by analyzing the velocity distribution function. This is a first attempt to understand the $\gamma \sim \beta$ relation and future research will hopefully give more insight into the nature of β (see [9]).

3.4 A prediction

As shown above most of the quantities are not very sensitive to the shape of the β profile. There is, however, one key prediction I want to show: It is possible to distinguish between isotropic and anisotropic velocity dispersions in structures. If $\beta = 0$ then equation (3.8) will reduce to,

$$\gamma_g = \gamma_{dm} , \quad (3.9)$$

which means that the dark matter and gas has to have the same shape. When the shapes of the dark matter profile and the gas profile are equal then the difference between the density profiles will only be a multiplicative factor, which in turn gives the prediction that the gas fraction should be a constant:

$$\beta = 0 \quad \Rightarrow \quad f_g = const . \quad (3.10)$$

The reverse is also true. $\gamma_g = \gamma_{dm}$ can only be fulfilled if the fraction $F_\beta = \frac{1}{1-\frac{2}{3}\beta}$ equals one. That is to say:

$$\beta \neq 0 \quad \Rightarrow \quad f_g \neq const . \quad (3.11)$$

There have been observations of many clusters with a non constant gas fraction (see e.g. [29]). Figure 3.4 shows a gas fraction where the different curves show different choices of the β profile, and it is clear that the $\beta = 0$ and the two non-zero profiles are very different. The $\beta = 0.2(\gamma + 0.8)$ curve has $\beta = 0.04$ towards the center which gives a more shallow gas fraction then the other curve which has $\beta = 0.13$ near the center.

This makes a compelling point against the assumption of $\beta = 0$, but I am not saying that the assumption of zero anisotropy should be completely abolished. In the center of relaxed clusters where we know that the anisotropy is small the assumption of $\beta = 0$ is still valid, but to assume that this is true for the structure as a whole is seldom a good approximation.

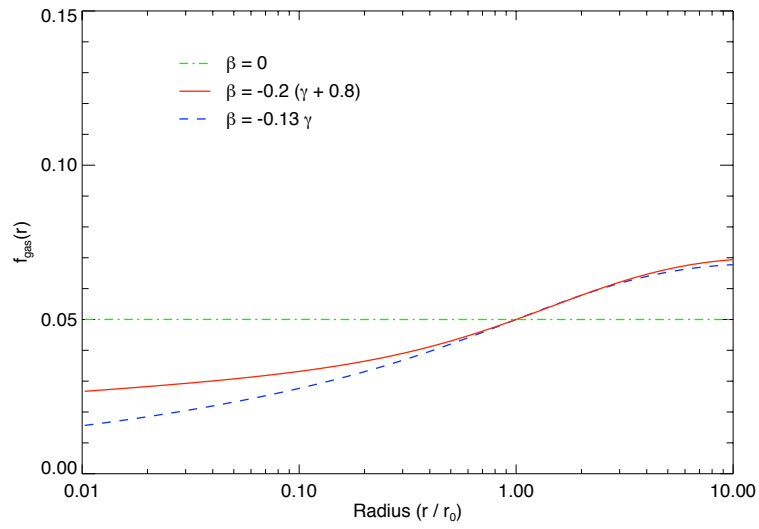


Figure 3.4: The gas fraction as a function of radius, assuming ρ_{dm} follows an NFW profile. Different curves are different β profiles. Note how $\beta = 0$ differs from the other two.

Chapter 4

Clusters of Galaxies

The method described in the last chapter together with the density profile for the dark matter forms a complete description of the gas in a galaxy cluster. I will use this fact to model the dark matter and predict observational quantities of the gas, which can be compared to observations. I will assume that the underlying dark matter profile can be parameterized by a Sersic/Einasto profile (described in section 2.4) or a generalized NFW (here after gNFW) with the inner slope as a free parameter. It is then possible to infer which choice of parameters and model (gNFW or Sersic) best fit the observations from the gas.

For illustrative purposes I will go through the treatment assuming a gNFW profile, but the full analysis was done both with a gNFW and a Sersic profile. The gNFW profile is given by,

$$\rho(r) = 2^{3-\gamma} \frac{\rho_0}{x^\gamma (1+x)^{3-\gamma}}, \quad \text{where } x = \frac{r}{r_0}. \quad (4.1)$$

The fitting parameters are the two scaling quantities r_0 , ρ_0 and the shape parameter γ which controls the inner slope of the profile.

4.1 Case Study: Abell 1689

The Abell 1689 Cluster (A1689 for short) is one of the clusters where we have excellent X-ray data and long exposure observations. Lensing observations have, however, shown that there is some clumping in the center of this cluster (see [19]), potentially departing from our assumption of spherical symmetry.

The usual way of determining the physical properties of a cluster is by observing the hot intra cluster gas in X-rays as described in sections 2.2. From the X-ray spectrum it is possible to find the temperature T and the density ρ of the gas. It is then possible to use the hydrostatic equilibrium equation

$$M(r) = \frac{k T r}{G \mu m_p} \left[\frac{d \ln T}{d \ln r} + \frac{d \ln \rho}{d \ln r} \right] \quad (4.2)$$

to find the total mass profile. When we have the total mass we can find the total density with $\rho = \frac{1}{4\pi r^2} \frac{dM}{dr}$, which will be dominated by dark matter, $\rho_{tot} = \rho_g + \rho_{dm} + \rho_* \approx \rho_{dm}$.

This would be the classic reduction method to determine the properties of the cluster from gas but we will here take another approach: We calculate an observable quantity from a proposed dark matter density, in this case surface brightness, and compare with observations. If the calculations do not fit the observations, we propose another dark matter density, until a good fit is found. This gives much better constraint on the parameters because we will be fitting to an observable with small error-bars and a high radial sampling. A general surface brightness profile will have 20-40 radial bins where a temperature profile will only have approximately 5-10 radial bins. The error-bars on the temperature profile will in general also be much larger and non trivial to improve, whereas the error-bars on the surface brightness are simply calculated via counting statistics (Poisson statistics).

The surface brightness is connected to the emissivity of the gas. The emissivity can be calculated from the gas properties and as shown in the previous chapters the gas properties are determined entirely by the dark matter distribution. For more details on that see the article in the appendix and for the detailed computation of the individual quantities see appendix A.4. Given a dark matter density we start by computing the mass profile, $M(r)$, and the slope, $\gamma_{dm}(r)$, of the density. From the slope we can determine the anisotropy $\beta(r)$ and when we have M , ρ and β we can compute the dispersion, $\sigma_r^2(r)$. It is the dispersion that can give us the gas temperature via

$$k T_g = \kappa \mu m_p \sigma_{dm}^2 = \kappa \mu m_p \sigma_r^2 (1 - \frac{2}{3} \beta) = \kappa \frac{\mu m_p \sigma_r^2}{F_\beta} \quad (4.3)$$

where kT is the temperature in units of keV and F_β is the beta factor (see appendix A.1). To continue we use the gas equation (3.8) to first give us the shape (slope) of the gas and then by solving a simple differential equation

($\frac{d \ln \rho}{d \ln r} = \gamma$), we get the gas density, ρ_g . This gas density has to be converted into the electron number density, n_e , by

$$n_e = \frac{\rho_g}{\mu_e m_p} \quad \text{where} \quad \mu_e = \frac{2}{1 + X}. \quad (4.4)$$

where μ_e is the electron mean molecular weight (see [4]), and X is the hydrogen abundance (just like Y is the helium abundance and Z is the abundance of heavy elements). This equation is valid as long as the gas is fully ionized.

When we have these quantities we can use the MeKaL model (see [21]) to compute how much each cm^3 is radiating. This radiance is computed

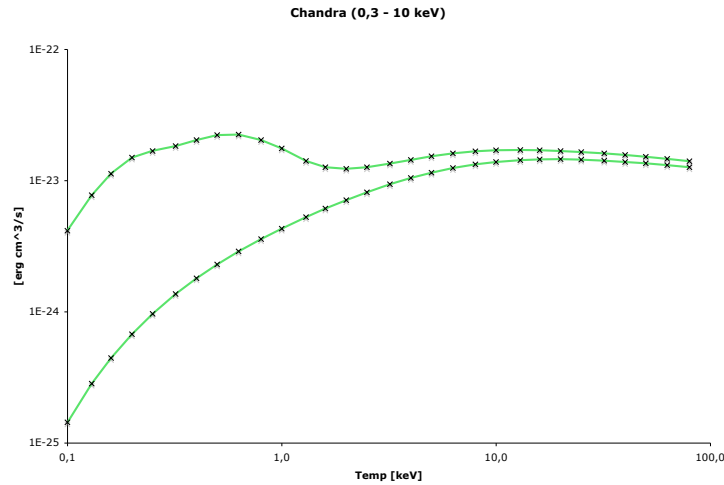


Figure 4.1: The "cooling function" $\Lambda(T) = \frac{\epsilon}{n_e^2}$ in $erg s^{-1} cm^3$ as a function of temperature, used to calculate how much each cm^3 is radiating. The lower curve is for zero metallicity and the upper is for solar metallicity. The points mark the tabulated values used in the program.

like $\epsilon = \Lambda(T) n_e^2$ where $\Lambda(T)$ is called the cooling function and tells you how much energy the gas is emitting depending on the temperature. The gas emits across the entire electromagnetic spectrum, but any scientific instrument is only able to register the radiation in some energy interval, so for our purpose we are only interested in the part that is emitted in the energies that our instrument is sensitive to, (for the extraction of $\Lambda(T)$ at specific energies see A.3). I extracted the profile by using an energy band pass like that of

the instrument of our observation in this case Chandra (see figure 4.1). The drawback of this approach is that $\Lambda(T)$ has to be updated each time the instrument or band-pass is changed because of the great sensitivity towards parameter (see appendix A.3).

When we have the emissivity profile, $\epsilon_{3d}(r)$, we first have to project our 3d model on to the sky plane. That is done with the projection integral, that looks like

$$\epsilon_{2d}(R) = \int_R^\infty \epsilon_{3d} \frac{r}{\sqrt{r^2 - R^2}} dr \quad (4.5)$$

where R is the projected radius on the sky plane and r is the 3d radius. Now we have how much one cm^2 on the sky emits. This quantity has to be converted to an observable surface brightness, Σ , with the equation,

$$\Sigma = \frac{dF}{d\Omega} = 3.74 \cdot 10^{-12} \frac{\epsilon_{2d}}{(1+z)^4}, \quad (4.6)$$

which has the unit of $erg\ s^{-1}\ cm^{-2}\ arcsec^{-2}$. For the derivation see appendix A.2. Figure 4.2 shows the surface brightness of Abell 1689, kindly provided by Signe Riemer-Sørensen (see [25]).

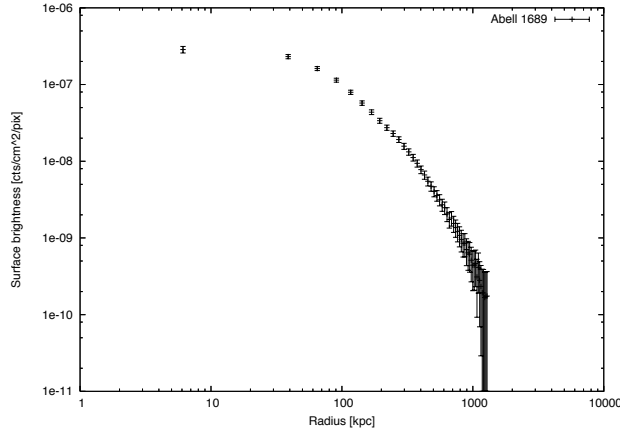


Figure 4.2: The surface brightness profile of Abell 1689, given in $count\ s^{-1}\ cm^{-2}\ pix^{-1}$ as a function of radius on logarithmic scale.

4.2 Results

The observational data that I have stems from [25]. In that paper the lower south-eastern half of the cluster is analyzed by itself because of the presence of some structure in the north-western half. The surface brightness data that we use is twice the south-eastern half, as shown in figure 4.2.

When given a density profile, we want to ensure that the radial profiles used internally in the method do agree with observations. This is part of a consistency check which let us gauge if the calculated surface brightness can be trusted. We will be using the NFW fit that was deduced in [25] as our input dark matter density for the dark matter. The fit is in general agreement with the results for A1689 from other people. We then compute the mass and temperature profile and compared this with the mass and temperature profile from the paper, as shown in figure 4.3 and 4.4. The mass profile agrees

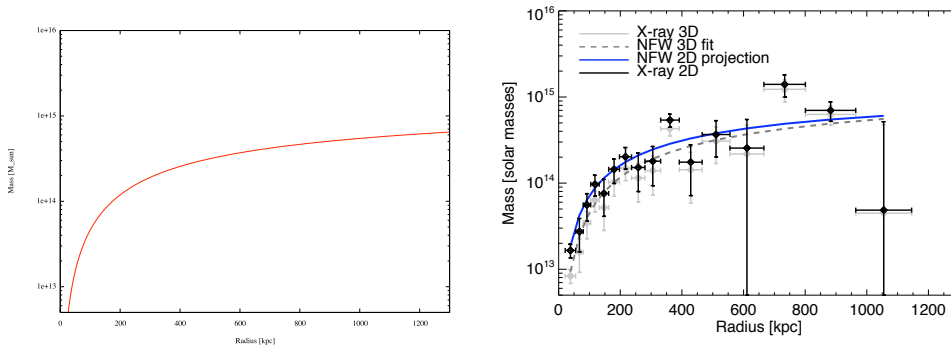


Figure 4.3: Left: The calculated mass profile from the fit given in [25]. Right: The mass profile derived in [25]. The y-axis is in solar masses, the x-axis is in kpc.

very well with the mass profile determined in the paper, but the temperature does not.

As seen in figure 4.4 the calculated temperature is too low compared to the observations. The temperature profile in the left panel is calculated with $\kappa = 1$ so the temperature profile reflects both the gas and the dark matter temperature.

Here there is observable evidence saying that $\kappa \neq 1$ for this cluster. But we can remedy that by recalling the definition of $\kappa = \frac{T_{dm}}{T_g}$ and adjusting it to the value dictated by the observational data. One could ask if this

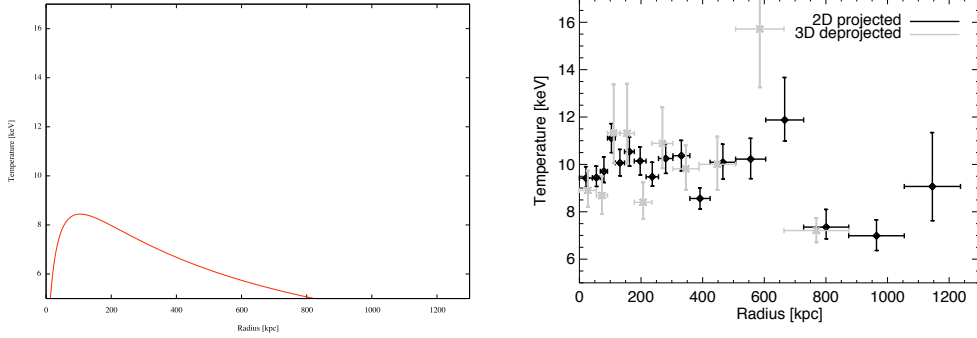


Figure 4.4: Left: The calculated temperature profile from the fit given in [25]. Right: The mass profile derived in [25]. The y-axis is the temperature in keV and the x-axis is in kpc.

low calculated temperature could be due to the breaking of one of the other assumptions, but as shown in chapter 3 the $\gamma \sim \beta$ does not affect the height of the temperature profile. A braking of the spherical symmetry assumption is only important in the central region and not at intermediate radii. Only an increase in the density will be able raise the temperature, but that would be inconsistent with the mass profile.

The departure from the DM temperature assumption implies that there is an energy source/sink. Since the dark matter temperature is lower than the gas temperature it means that there is an input of energy to the gas that does not comes from the dark matter. The explanation is probably connected to the X-ray feature in the north-western half of the cluster. This could either be a source emitting energy directly into the gas¹ or it could be some sort of merging structure exerting a ram pressure on the cluster thereby heating the gas. Both these scenarios would make $\kappa < 1$ as is observed here.

We remedy this by adjusting $\kappa = 0.7$ according to the observation which will enable us to continuing our analysis of the cluster.

The calculated surface brightness given $\kappa = 0.7$ is shown in figure 4.5. It is worth noting that this is not a fit to the surface brightness. The proposed dark matter density profile is a generic NFW fit obtain through a classical reduction of X-ray data (see [25]).

The next step will be to device a fitting program to fit the surface bright-

¹A source like an AGN or such would probably already had been identify as a such, which makes this explanation the least likely of the two.

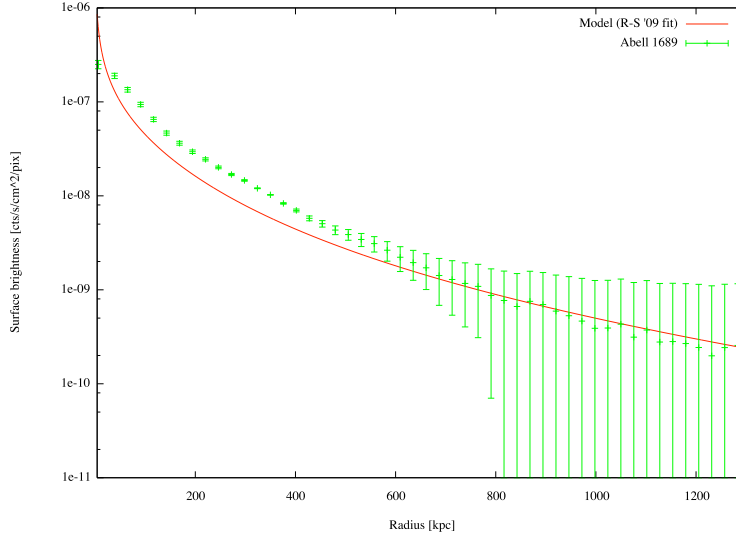


Figure 4.5: The surface brightness profile of Abell 1689, given in $\text{count s}^{-1} \text{cm}^{-2} \text{pix}^{-1}$ as a function of radius on linear scale. The solid line is the calculated surface brightness from the NFW fit in [25]

ness with the gNFW and Sersic profile, it is my plan to do so in the future. If this turns out to be successful I would like to extend the program to take a free density profile with as many discrete data point as the surface brightness profile.

I was able to manage a preliminary investigations by doing simple fitting by hand. This revealed that the generated surface brightness profiles were not flat enough towards the center. Only for cored (or very mildly cusped) density models the slope of the surface brightness approached the slope of the observational data.

If a general surface brightness resembles a beta model (see [2]) it will be flat towards the center. There are three ways of making the surface brightness flat: The simplest way is to have a cored density profile, but this would imply that a great fraction of the observed clusters would have a cored or only mildly cusped dark matter density. If a cored dark matter density is not the explanation then it is possible to make the surface brightness more flat by putting less (the is negative) β in the center, whereby the dispersion becomes tangentially biased. This is potentially in conflict with numerical

simulations. The last way of making the surface brightness flat is by letting κ depart from unity.

These concerns towards a flat surface brightness in a cusped dark matter potential have to be investigated in the future, through X-ray observations of relaxed spherical unperturbed clusters.

Chapter 5

Summary

5.1 Conclusion

I have in this thesis introduced a new method for determining the properties of galaxy clusters. With this method it is possible to derive the dark matter density from the gas properties, in particular the surface brightness profile. Other people have looked at similar approaches, like assuming that the phase-space density is a perfect power law (see [6]) but it is doubted whether the phase-space density is a universal power law (see [27]). Others again have assumed that the gas entropy profile has a certain shape (see [3]), but there is in the scientific community not yet consensus on the shape of the entropy profile or whether it is universal or not.

The approach in this thesis is relying on four assumptions. The first two are The Jeans equation and the hydrostatic equilibrium which are both very well tested. The two other assumptions come from numerical simulations where a linear correlation between the dark matter density slope, γ , and the velocity anisotropy, β , (the $\gamma \sim \beta$ relation), has been confirmed (see e.g. [12]). The last assumption is the dark matter temperature relation, where it has been shown that $\kappa = \sigma_{dm}^2/\sigma_g^2$ is very close to unity (1.0 ± 0.1 , see [14]).

I show in chapter 3 that given a dark matter density all the physical properties of the gas can be computed from the dark matter distribution alone. I also show that the different choices of $\gamma \sim \beta$ do only influence the different radial profiles to a small degree.

In chapter 4 this knowledge is turned into a fitting method. The advantage of this method is that I am able to fit to an observable where the error

bars are small and the sampling is large. The surface brightness profile will typically consist of 20-40 radial bins as opposed to the temperature profile which typically only have 5-10 bins, so an increase of the radial sampling of at least three times is not unusual. The error-bars on the surface brightness can be improved by taking longer exposures as oppose to the temperature, where improving the error-bars is harder. Since the temperature, gas density and gas fractions profiles can be considered side effects of the method they can be used to check if the assumptions hold and for that a high radial resolution is not needed. In chapter 4, I demonstrated how this consistency check can improve the assumptions if a particular cluster is inconsistent with the data. Here the problem was the κ assumption, where an adjustment ($\kappa = 0.7$) resulted in an fairly acceptable alignment to the data.

It is important to note here that this new method is not intended to replace current models and methods. This method is intended to give better constraint on the shape of the dark matter density shape by reducing systematic errors in the reduction process. It is also worth noting that this method only works properly on relaxed spherically symmetric cluster.

5.2 Outlook

Now my plan is to run a Monte Carlo code trough the parameterized density models to determine the best fitting density profile and expand my analysis to more clusters. For example to investigate if a cluster has a core or a cusp or to see if a Sersic or a gNFW is a better fit. This analysis can then be extended to a free density profile that should contain as many discrete point as the surface brightness profile and thereby give a radial density profile free of any density model interpretation. All the other radial profiles that can be calculated from the dark matter density can also be inferred in this way.

But there is also the opportunity to investigate the assumptions further. If we analyze clusters where we know all the radial profiles with high enough precision we can investigate if the $\gamma \sim \beta$ relation really behaved as in the simulations or if κ really is close to unity as we approach the center. The opportunity for confirming a result seen in numerical simulation by observational means is present.

Also the behavior of κ in the presence of a cD galaxy or AGN engine in the center and how it correlates with the properties of those would be of high scientific value.

As a last notion I want to mention that when the dark matter density profile is known then this can be compared to independent methods like lensing or even kinematic studies of the line-of-sight velocities of the individual galaxies.

Appendix A

Equations

Through out this thesis equations are used extensively. Therefore, I have put the derivations into the appendix on the following pages.

A.1 The gas equation

In this section I will derive the main equation in chapter 3, *the gas equation*. The two most important governing equations in this treatment is the Jeans equation and the Hydrostatic Equilibrium. These exist in many forms, but the form used here clearly shows how similar they are:

$$\frac{GM(< r)}{r} = -\frac{k_B T}{G\mu m_p} \cdot \left[\frac{d \ln \rho_g}{d \ln r} + \frac{d \ln T}{d \ln r} \right] + \frac{r^2 v_r}{G} \frac{dv_r}{dr} - \frac{r \cdot v_{rot}^2}{G}, \quad (\text{A.1})$$

$$\frac{GM(< r)}{r} = -\sigma_r^2 \cdot \left[\frac{d \ln \rho_m}{d \ln r} + \frac{d \ln \sigma_r^2}{d \ln r} + 2\beta \right] \quad (\text{A.2})$$

Here $M(< r)$ is the mass interior to r , ρ_g is gas density, ρ_m is total matter density, v_r is radial bulk motion (in-fall negative, outflow positive), $v_{rot}^2 = v_\phi^2 + v_\theta^2$ is bulk rotation. We start by rearranging the equation like this

$$\frac{k_B T}{G\mu m_p} \cdot r \cdot \left[\frac{d \ln T}{d \ln r} + \frac{d \ln \rho_g}{d \ln r} \right] = \frac{\sigma_r^2 \cdot r}{G} \cdot \left[\frac{d \ln \rho_m}{d \ln r} + \frac{r v_r}{\sigma_r^2} \frac{dv_r}{dr} - \frac{v_{rot}^2}{\sigma_r^2} + \frac{d \ln \sigma_r^2}{d \ln r} + 2\beta \right], \quad (\text{A.3})$$

to collect all the non pressure terms. From this we define a new parameter, the effective density slope γ_e as

$$\gamma_e = \frac{d \ln \rho_m}{d \ln r} + \frac{r v_r}{\sigma_r^2} \frac{dv_r}{dr} - \frac{v_{rot}^2}{\sigma_r^2}. \quad (\text{A.4})$$

Which gives

$$\frac{k_B T}{\mu m_p} \cdot \left[\frac{d \ln T}{d \ln r} + \frac{d \ln \rho_g}{d \ln r} \right] = \sigma_r^2 \cdot \left[\gamma_e + \frac{d \ln \sigma_r^2}{d \ln r} + 2\beta \right] \quad (\text{A.5})$$

The motivation for introducing this new parameter is that all the terms concerning rotation, radial in-fall and other non-pressure terms are now confined to this one parameter. In the customary derivation of the hydrostatic equilibrium it is assumed that the system is not rotating and radial in-fall (or outflow) is negligible.

I have hereby shown that the case of non-vanishing bulk motion can be transformed into the case of no bulk motion and only thermal pressure by absorbing the non-vanishing terms into the density parameter. This trick, however, is purely theoretical because γ_e no longer represents the shape of the dark matter density.

From this point on I will assume that all the non-thermal and bulk motion terms are negligible and continue in the classical treatment, whereby $\gamma_e = \gamma_{dm} \equiv \gamma$.

Now we continue with the introduction of the dark matter temperature, which is defined as

$$\sigma_{dm}^2 = \kappa \cdot \sigma_{gas}^2, \quad \text{where} \quad \sigma_{dm}^2 = \frac{1}{3}(\sigma_r^2 + \sigma_\theta^2 + \sigma_\phi^2) \quad \text{or} \quad (\text{A.6})$$

$$T_{dm} = \kappa \cdot T_{gas}, \quad \text{where} \quad \frac{k_B T_{dm}}{\mu m_p} = \sigma_{dm}^2. \quad (\text{A.7})$$

This is then inserted into equation (A.5) to cancel out the gas temperature like this:

$$\frac{\sigma_{dm}^2}{\kappa} \cdot \left[\frac{d \ln \kappa^{-1} \sigma_{dm}^2}{d \ln r} + \frac{d \ln \rho_g}{d \ln r} \right] = \sigma_r^2 \cdot \left[\gamma + \frac{d \ln \sigma_r^2}{d \ln r} + 2\beta \right]. \quad (\text{A.8})$$

After some algebra and use of the definition of the $\sigma_{dm}^2 = \sigma_r^2(1 + \frac{2}{3}\beta)$ the above equation becomes

$$\gamma_g = \frac{d \ln \rho_g}{d \ln r} = \frac{1}{1 - \frac{2}{3}\beta} \left[\kappa(\gamma + 2\beta) + \left(\frac{2}{3}\beta + \kappa - 1\right) \frac{d \ln \sigma_r^2}{d \ln r} - \frac{2}{3} \frac{d\beta}{d \ln r} \right] + \frac{d \ln \kappa}{d \ln r}. \quad (\text{A.9})$$

From [14] we know that κ can be approximated very well with a constant of 1.0 ± 0.1 , so I will assume $\kappa = 1$ which simplifies the above equation to

$$\gamma_g = \frac{1}{1 - \frac{2}{3}\beta} \left[\gamma + 2\beta + \frac{2}{3}\beta \frac{d \ln \sigma_r^2}{d \ln r} - \frac{2}{3} \frac{d\beta}{d \ln r} \right]. \quad (\text{A.10})$$

The fraction in the front turns up a few times in the equations so I will define a shorthand, which I will call the beta factor

$$F_\beta = \frac{1}{1 - \frac{2}{3}\beta}. \quad (\text{A.11})$$

The interpretation of F_β can be summarized like this:

β	F_β	Description
1	3	Radial dominated
0	1	Isotropic
$-\infty$	0	Tangential dominated

This makes the final gas equation look like this

$$\gamma_g = F_\beta \cdot \left[\gamma + 2\beta + \frac{2}{3}\beta \frac{d \ln \sigma_r^2}{d \ln r} - \frac{2}{3} \frac{d\beta}{d \ln r} \right]. \quad (\text{A.12})$$

A.2 Surface brightness

Here I give the derivation of how to convert emissivity to surface brightness, where surface brightness is defined as *flux per solid angle*,

$$\Sigma = \frac{dF}{d\Omega}. \quad (\text{A.13})$$

Beside the definition of surface brightness we also need these three basic definitions:

$$dA = d_a^2 d\Omega \quad (\text{A.14})$$

$$dL = 2 \epsilon_{2d} dA \quad (\text{A.15})$$

$$dF = \frac{dL}{4\pi d_l^2} \quad (\text{A.16})$$

where ϵ_{2d} is the 2d emissivity, d_a and d_l is the angular diameter and luminosity distance respectively. dL is the luminosity that we receive as flux dF per area dA from the solid angle $d\Omega$. The reason for the constant "2" in equation A.15 is that after the emissivity has been projected we only receive the photons that are sent towards us and not away from us, so the total luminosity will be

twice the amount in our direction. We now put the three equations together to gives us:

$$dF = \frac{2 \epsilon_{2d} dA}{4\pi d_l^2} = \frac{2 \epsilon_{2d} d_a^2 d\Omega}{4\pi d_l^2} \quad (\text{A.17})$$

This is then inserted in the definition of surface brightness, but we also need the fact that

$$\frac{d_l}{d_a} = (1 + z)^2. \quad (\text{A.18})$$

Using this fact makes the surface brightness independent of distance and cosmology and therefore an intrinsic property of the source. The final equations looks like:

$$\Sigma = \frac{\epsilon_{2d}}{2\pi (1 + z)^4}. \quad (\text{A.19})$$

This has the same unit as ϵ_{2d} times rad^{-2} . If we want to convert it to $arcsec^{-2}$ we have to divide by $606265 arcsec/rad$ to give:

$$\Sigma = 3.74 \cdot 10^{-12} \frac{\epsilon_{2d}}{(1 + z)^4}. \quad (\text{A.20})$$

If the surface brightness is calculated per pixel we can convert this if we know the pixel-size, L_{pix} . If L_{pix} is measured in $arcsec/pix$ then the surface brightness becomes:

$$\Sigma = 3.74 \cdot 10^{-12} \frac{\epsilon_{2d}}{(1 + z)^4} L_{pix}^2. \quad (\text{A.21})$$

A.3 The MeKaL model

The name MeKaL is an acronym for Mewe-Kaastra-Liedahl. Rolf Mewe et al. calculated the atomic data for a hot optical thin plasma in 1985, Jelle S. Kaastra then wrote the first code for fitting from these data in 1992 and Duane A. Liedahl et al. improved the data for the Fe lines in 1995. This model is one of the most used models when fitting spectral data today and is a standard model in software packages like Xspec.

The MeKaL model that is used in this thesis is the Xspec implementation and it takes a number of input parameters like: temperature, heavier elements abundance, hydrogen density and a normalization factor. I will call the set of input parameters, $par = \{n_H, Z, z, Norm, (E_0, E_1)\}$, which also contains the energy interval of the observation.

The amount of radiation that a volume of gas outputs is given by the emissivity $\epsilon = \Lambda(T) n^2$, where n^2 is the number density of the gas inside the volume we are looking at. The functional form $\Lambda_{par}(T)$ that I want to extract must be a function of temperature alone. That means that I need to fix the input parameters par , so that Xspec will output $\Lambda(T)$ and so that the values makes sense for the specific combination of instrument and source. But first we take a look at the definition of Λ :

$$\Lambda = \frac{L}{n_e^2}, \quad (\text{A.22})$$

which has the unit of energy per second times volume or $erg\ cm^3\ s^{-1}$ or even $photons\ cm^3\ s^{-1}$. Xspec calculates the flux from a model spectrum $M(E)$ like,

$$F = \frac{1}{E_1 - E_0} \int_{E_0}^{E_1} M(E) dE. \quad (\text{A.23})$$

This has the unit of either $erg\ cm^{-2}\ s^{-1}$ or $photons\ cm^{-2}\ s^{-1}$. And now we want to turn flux into luminosity pr electrons squared:

$$\Lambda_{par} = \frac{L}{n_e^2} = \frac{4\pi d_l^2 F}{n_e^2} \quad (\text{A.24})$$

For a specific combination of parameter par Xspec calculated the flux like:

$$F_{par} = \frac{Norm}{E_1 - E_0} \int_{E_0}^{E_1} f(E) dE. \quad (\text{A.25})$$

where $Norm$ and E_0, E_1 are the normalization and energy band parameters in $par = \{n_H, Z, z, Norm, (E_0, E_1)\}$ and $f(E)$ is the functional form of the spectrum that Xspec calculates. In the documentation of Xspec it is stated how $Norm$ should be interpreted:

$$Norm = \frac{10^{-14} \int n_e n_H dV}{4\pi d_a^2 (1+z)^2}. \quad (\text{A.26})$$

Inserting that into equation (A.24) gives:

$$\Lambda_{par} = 10^{-14} (1+z)^2 \frac{\int n_e n_H dV}{n_e^2} \frac{\int_{E_0}^{E_1} f(E) dE}{E_1 - E_0} \quad (\text{A.27})$$

where I have used that $\frac{d_i}{d_a} = (1+z)^2$. Let us have a closer look at the three factors. The factor

$$10^{-14}(1+z)^2 \quad (\text{A.28})$$

is a constant factor and the redshift dependence. We set the redshift to zero as we want to know how much a cubic centimeter radiates in the local frame. The factor

$$\frac{\int n_e n_H dV}{n_e^2} \approx \frac{n_H}{n_e} \Delta V = \frac{2X}{1+X} \Delta V \quad (\text{A.29})$$

contains all the density terms. As we are only interested in a small volume lets say $\Delta V = 1 \text{cm}^3$ the approximation turns this term into a ratio. This ratio can be rewritten by using $n_H = X \frac{\rho}{m_p}$ and $n_e = \frac{\rho}{m_p} \frac{1+X}{2}$ to give the last expression, where X is the abundance (in mass) of Hydrogen (like Y is for Helium and Z is for the heavier elements). This term is $0.80 - 0.88$ for $X = 0.66 - 0.80$. The last term

$$\frac{\int_{E_0}^{E_1} f(E) dE}{E_1 - E_0} \quad (\text{A.30})$$

is the MeKaL models dependence on energy. This is the integral we need to let Xspec do over all the energy range that our instrument can observe. It is actually this integral that makes the shape of $\Lambda(T)$ instrument dependent, and this is why we have to extract a new $\Lambda(T)$ if we change instrument. This integral depends on the energy band chosen and even on the response function of the individual instrument if we use *photon* as the energy unit.

After this thorough discussion, we are able to choose a suitable set of parameters to extract $\Lambda(T)$ from the Xspec MeKaL model: Temperature is the free parameter that we want the functional dependence of. E_0, E_1 will depend on the instrument used (and maybe even on the reduction method if hard energy cuts have been used). The redshift we need to put to zero and the normalization parameters $Norm = 0.8 \cdot 10^{-14}$ for almost all realistic choices of hydrogen content. For the metallicity dependence it turns out that it scales like,

$$\Lambda(T, Z) = \Lambda(T, 0) \left(\frac{\Lambda(T, Z_\odot)}{\Lambda(T, 0)} \right)^{Z/Z_\odot}. \quad (\text{A.31})$$

From this equation we see that we only need $\Lambda(T, Z_\odot)$ and $\Lambda(T, 0)$ to get $\Lambda(T)$ for any metallicity. So by choosing these particular parameter we

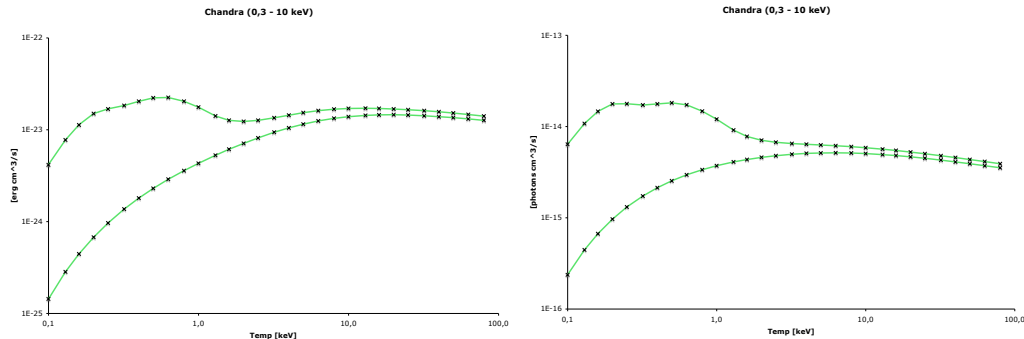


Figure A.1: The $\Lambda(T)$ function extracted from Xspec’s MeKaL model. Upper curves are for solar abundance gas lower curves are for gas with zero abundance. The points marked are the values extracted. The intermediate points are interpolated. Left: Energy unit, $erg\ cm^3\ s^{-1}$. Right: Energy unit, $photons\ cm^3\ s^{-1}$.

make Xspec output $\Lambda(T, Z_{\odot})$ or $\Lambda(T, Z_{\odot})$ directly in the unit $erg\ cm^3\ s^{-1}$ or $photons\ cm^3\ s^{-1}$.

The shape of $\Lambda(T)$ is shown for the Chandra satellite in the energy interval $0.3 - 10\ keV$ in the two different energy units in figure A.1. The two curves in each plot show $\Lambda(T)$ for two different metallicities. The lower one is for zero metallicity where all the emissions from the gas comes from the continuum (bremsstrahlung), whereas the upper one is for solar metallicity and shows features especially at the low temperatures, which stems from the larger fraction of emission from the emission lines. All intermediate metallicities $\Lambda(T)$ will lie between the two curves (see equation (A.31)). A typical metallicity for clusters will be a third solar, which gives that a typical $\Lambda(T)$ will lie a third way up from the lower curve.

A.4 IDL-implementation

The problem in dealing with equations like those that arise from the Jeans equation and the logarithmic slopes is that they are seldom nice functions or at least analytical. So often we are forced to do all calculations numerically. In this thesis I will be doing most of the numerical analysis in the IDL language.

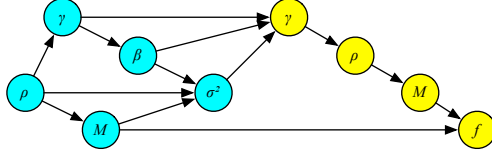


Figure A.2: Calculation flow diagram. Left are the DM-quantities, right the gas quantities.

The diagram below shows what quantities will be calculated in what order (left to right).

This method takes a **density** profile as input and calculates all other quantities from that. The density will be stored as an array of 1000 floating-point numbers. Together with a *radius array* this makes out the density profile. The radius is logarithmically spaced over four orders of magnitudes from $10^{-2}r_0$ to 10^2r_0 , where r_0 is a reference radius. The radius interval contains only intermediate radii and does not go all the way to zero.

In the next paragraphs I will go through each step indicated in figure A.2 and describe how each quantity is computed. The general notation is that x_i will represent an element in the radius array, $y_i = y(x_i)$ is an input profile like the density, mass or slope profile and $f_i = f(x_i)$ will be the output profile that the particular calculation will return.

First the **logarithmic density slope**, γ , is calculated numerically from the density profile via the equation,

$$\gamma = \frac{d \ln \rho}{d \ln r}. \quad (\text{A.32})$$

I discretize the derivative by using the point in front and behind the current point to calculate the slope,

$$\left. \frac{d \ln y}{d \ln x} \right|_i = \frac{\ln y_{i+1} - \ln y_{i-1}}{\ln x_{i+1} - \ln x_{i-1}} = \frac{\ln \frac{y_{i+1}}{y_{i-1}}}{\ln \frac{x_{i+1}}{x_{i-1}}}. \quad (\text{A.33})$$

This is a second order method¹. At the endpoints I have to use i instead of $i \pm 1$.

¹”Second order” means that increasing the number of points x times makes the error go down by x^{-2} .

The **mass**, M , is also calculated numerical from the density profile with the integral,

$$M(r) = \int_0^r 4\pi\tilde{r}^2\rho(\tilde{r}) d\tilde{r}. \quad (\text{A.34})$$

This integral is discretized like

$$f_i = f(x_i) = \int_{x_0}^{x_i} y(\tilde{x}) d\tilde{x} = f_{i-1} + \frac{1}{2}(y_i + y_{i-1})(x_i - x_{i-1}) \quad (\text{A.35})$$

which is the trapezoid method and also a second order method. Our radius does not go all the way to zero, so our problem lies in finding the initial condition $f_0 = f(x_0)$ which starts the sequence. And for that I assume that the first few point of f should follow a power-law (i.e. a straight line on log-log-scale). This then gives the following form for f_0

$$f_0 = f(x_0) = \frac{y_0 x_0}{\gamma_0 + 1} \quad \text{where} \quad \gamma = \frac{d \ln y}{d \ln x} \quad (\text{A.36})$$

The derivation can be seen in appendix A.5. This has the advantage that if the input profile does not have any features outside our radial interval, then we don't need to know the value of the integral outside our interval.

The **velocity anisotropy**, β , is calculated from the density slope, given a $\gamma \sim \beta$ relation (see [9], [11], and [12]),

$$\beta(r) = A\gamma(r) + B, \quad (\text{A.37})$$

where the constants A and B are determined from numerical simulations of halo formation. If nothing else is mentioned I use the values: $A = 0.2$ and $B = 0.16$ (see [12])

To calculate **the radial velocity dispersion** σ_r^2 we rewrite the Jeans equation to

$$\sigma_r^2(r) = \frac{1}{\tilde{\rho}(r)} \int_r^\infty \frac{G M(\tilde{r}) \tilde{\rho}(\tilde{r})}{\tilde{r}^2} d\tilde{r} \quad \text{where} \quad \frac{d \ln \tilde{\rho}}{d \ln x} = \gamma + 2\beta \quad (\text{A.38})$$

If the velocity anisotropy had been zero $\tilde{\rho}$ would equal the density ρ . But since β is generally nonzero we have to correct for that with $\tilde{\rho}$. To find $\tilde{\rho}$ we have to solve the equation

$$\frac{d \ln f}{d \ln x} = y \quad (\text{A.39})$$

by discretizing the derivative like in equation (A.33). After some rearranging it looks like this

$$f_{i+1} = f_{i-1} \left(\frac{x_{i+1}}{x_{i-1}} \right)^{y_i} \quad (\text{A.40})$$

The choice of f_0 will only be a multiplying factor and since $\tilde{\rho}$ appears both in the numerator and the denominator of equation (A.38) any multiplying factor will cancel out. So any choice of f_0 on $\tilde{\rho}$ will never affect the calculation of σ_r^2 . For the numerical calculation of the integral I swap the boundaries and reuse the algorithm from equation (A.35) with the same choice of f_0 .

The calculation of **the gas density slope**, γ_g is straight forward insertion in the definition of γ_g

$$\gamma_g = \frac{1}{1 - \frac{2}{3}\beta} \left(\gamma_{dm} + 2\beta + \frac{2}{3} \frac{d \ln \sigma_r^2}{d \ln r} + \frac{2}{3} \frac{d\beta}{d \ln r} \right) \quad (\text{A.41})$$

where the derivatives are calculated as in equation (A.33)

The gas density, ρ_g is calculated like $\tilde{\rho}$, by solving $\frac{d \ln \rho_g}{d \ln r} = \gamma_g$, where the choice of f_0 will give a multiplicative factor. This translate physically to how much gas is in the system.

The gas fraction, f_g is given by the definition

$$f_g = \frac{M_g}{M_{tot}} = \frac{M_g}{M_{dm} + M_g} \quad (\text{A.42})$$

and is a calculable quantity, since M_g and M_{dm} is known from above.

A.5 Numerical integration

The following integral comes up during the calculations of some of the quantities, but because the radial interval is not going all the way from zero to infinity like some of the integrals that are to be evaluated, I have to "guess" the value of the part of the integral that is outside our interval.

$$f_i = f(x_i) = \int_{x_0}^{x_i} y(\tilde{x}) d\tilde{x} = f_{i-1} + \frac{1}{2}(y_i + y_{i-1})(x_i - x_{i-1}) \quad (\text{A.43})$$

If the wrong f_0 is chosen the first f_i 's will be off, until the sequence catches up and is no longer dominated by the first few (wrong) term. For that reason i need to guess f_0 close enough to the true value the integral would have had

if we had taken the part outside our interval into account. I have chosen the condition that the first few f_i 's should follow a power law because this is not too far from what we see in the plots of these quantities.

To calculate what f_0 has to be if $f(x)$ is a power law we assume that the first few points of y_i follow a power law. This is a good first approximation for the majority of the quantities in the calculations.

$$y \approx x^\gamma \quad \text{for} \quad x \approx x_0 \tag{A.44}$$

Then we solve the integral straight-forward:

$$\int x^\gamma dx = \frac{x^{\gamma+1}}{\gamma+1} = \frac{y x}{\gamma+1} \tag{A.45}$$

because $x^{\gamma+1} = x^\gamma x = y x$. So now we have a guess for f_0 like this:

$$f_0 = \frac{y_0 x_0}{\gamma_0 + 1} \tag{A.46}$$

where γ_0 is an estimate of the log-slope of y_i at x_0 . So even if y_i is not a powerlaw the approximation still makes sense, as long as γ is only slowly changing inside a small enough interval around x_0 .

Appendix B

Article

The following pages contain an article that has been submitted to The Astrophysical Journal. The article is as of April 30, 2009 in second peer review, after a positiv first referee report.

Determining all gas properties in galaxy clusters from the dark matter distribution alone

Teddy F. Frederiksen[†], Steen H. Hansen[†], Ole Host[†], Marco Roncadelli[‡]

[†] *Dark Cosmology Centre, Niels Bohr Institute, University of Copenhagen,
Juliane Maries Vej 30, 2100 Copenhagen, Denmark*

[‡] *INFN, Sezione di Pavia, Via A. Bassi 6, 27100 Pavia, Italy*

ABSTRACT

We demonstrate that all properties of the hot X-ray emitting gas in galaxy clusters are completely determined by the underlying dark matter (DM) structure. Apart from the condition of hydrostatic equilibrium for the gas and the Jeans equation for the DM, our proof is based on two simple relations which have recently emerged from numerical simulations: the equality of the gas and DM temperatures, and the almost linear relation between the DM velocity anisotropy profile and its density slope. For DM distributions described by the NFW or the Sersic profiles, the resulting gas density profile, the gas-to-total-mass ratio profile, and the entropy profile are all in good agreement with X-ray observations. Our result allows us to predict the X-ray luminosity profile of a cluster in terms of its DM content alone. As a consequence, a new strategy becomes available to constrain the DM morphology in galaxy clusters from X-ray observations. Our results can also be used as a practical tool for creating initial conditions for realistic cosmological structures to be used in numerical simulations.

Subject headings: dark matter, galaxies: clusters: general, X-rays: galaxies: clusters

1. Introduction

Galaxy clusters are the largest equilibrated structures in the Universe, consisting mainly of dark matter (DM) and hot ionized gas in hydrostatic equilibrium in the overall potential well. Observations of this X-ray emitting gas allow for an accurate determination of the properties of the dominating DM structure, which can then be compared with the results of numerical N-body simulations.

More specifically, the strategy can be outlined as follows. In the first place, the equation of hydrostatic equilibrium can be used to infer the DM density profile from X-ray data (Fabricant et al. 1980). Application of this technique in conjunction with present-day observations (Voigt & Fabian 2006; Pointecouteau et al. 2005) yields density profiles which are in excellent agreement with those emerging from numerical simulations of structure formation (Navarro et al. 1996; Moore et al. 1998; Die-

mand et al. 2004; Stadel et al. 2008; Navarro et al. 2008). Moreover, using a very simple connection between the gas and DM temperatures which has been confirmed by numerical simulations, the equation of hydrostatic equilibrium can be combined with the Jeans equation for the DM to derive both the DM radial velocity dispersion and the velocity anisotropy profile (Hansen & Piffaretti 2007; Host et al. 2009). Again, the resulting profiles turn out to be in excellent agreement with numerical simulations (Cole & Lacey 1996; Carlberg et al. 1997).

Measurements of the gas temperature profile have demonstrated its virtually universal properties (De Grandi & Molendi 2002; Kaastra et al. 2004; Vikhlinin et al. 2005; Pointecouteau et al. 2005; Voigt & Fabian 2006). This universality appears surprising since the temperature profile should encode information about the violent gravitational processes taking place during the cluster formation, as well as any additional en-

ergy input, e.g. from a central heat engine, and these processes are expected to differ significantly from structure to structure. The gas density profile also exhibits a roughly universal behaviour, which has allowed observers to fit remarkably simple forms, e.g. a beta-profile (Cavaliere & Fusco-Femiano 1976; Sarazin 1986), to the data.

A natural question arises as to whether the properties of the hot X-ray emitting gas in galaxy clusters can be *predicted* from first principles starting from the cluster DM distribution alone. Attempts in that direction have been performed in the past (Makino et al. 1997; Suto et al. 1998), under the assumption that the gas can be treated either as isothermal or polytropic. Unfortunately, later observations have shown that these assumptions are incorrect.

Below, we will show how the gas density profile can be obtained directly from the underlying DM profile, by combining the equation of hydrostatic equilibrium for the gas and the Jeans equation for the DM. Besides the above-mentioned relation between the gas and DM temperatures, our derivation rests upon a very simple connection between the DM velocity anisotropy and the slope of its density profile, which has recently emerged in numerical simulations (Hansen & Moore 2006; Hansen & Stadel 2006). We thereby demonstrate that the gas density profile is completely determined once the gravitationally dominant DM density profile is given. Since the gas temperature profile is also known, it turns out that the DM distribution dictates all the gas properties *uniquely*. Besides conceptually relevant in itself, this fact allows to predict the X-ray luminosity profile of a cluster in terms of its DM content alone. So, a new strategy becomes available to constrain the DM morphology in galaxy clusters from X-ray observations. Moreover, our findings can be employed as a practical tool for creating initial conditions for realistic cosmological structures to be used in numerical simulations.

2. Background

We start by recalling some basic information which will be instrumental for our analysis. We restrict our attention throughout to regular clusters, which are supposed to be spherically symmetric and relaxed. The condition of hydrostatic

equilibrium for the X-ray emitting gas can be written as

$$\frac{k_B T_g}{\mu m_p} \left(\frac{d \ln \rho_g}{d \ln r} + \frac{d \ln T_g}{d \ln r} \right) + \frac{GM_{\text{tot}}(r)}{r} = 0, \quad (1)$$

where $\rho_g(r)$ and $T_g(r)$ are the gas density and temperature profiles, respectively, $\mu \simeq 0.61$ is the mean molecular weight for the intracluster gas, m_p is the proton mass and $M_{\text{tot}}(r)$ represents the total mass inside radius r . Two conditions have to be satisfied in order for Eq. (1) to hold. First, it should be applied to a region considerably larger than the gas mean free path, so that local thermodynamic equilibrium is established. Second, the cooling time in that region should be larger than the age of the cluster, so that no bulk motion occurs. The latter condition is generally met outside the central region, where the presence of a cooling flow often requires Eq. (1) to be replaced by the Euler equation (with the velocity term playing a nonnegligible role). Because of collisional relaxation, the gas velocity distribution is isotropic and its temperature can be expressed in terms of the one-dimensional velocity dispersion σ_g^2 as

$$T_g = \frac{\mu m_p \sigma_g^2}{k_B}. \quad (2)$$

Assuming complete spherical symmetry for the DM distribution, the two tangential components of the DM velocity dispersion, denoted by σ_t^2 , are necessarily equal, but they are generally allowed to differ from the radial component σ_r^2 , since DM is supposed to be collisionless. It is usual to quantify the DM velocity anisotropy by

$$\beta \equiv 1 - \frac{\sigma_t^2}{\sigma_r^2} \quad (3)$$

and we find it convenient to introduce the mean DM one-dimensional velocity dispersion σ_{DM^2} as

$$\sigma_{\text{DM}^2}^2 \equiv \frac{1}{3} (\sigma_r^2 + 2\sigma_t^2) = \left(1 - \frac{2}{3}\beta \right) \sigma_r^2. \quad (4)$$

Moreover, in analogy with the case of a gas, we also define the DM temperature as Hansen & Piffaretti (2007)

$$T_{\text{DM}} \equiv \frac{\mu m_p \sigma_{\text{DM}^2}^2}{k_B} = \frac{\mu m_p}{k_B} \left(1 - \frac{2}{3}\beta \right) \sigma_r^2. \quad (5)$$

Of course, the collisionless nature of DM prevents any definition of temperature in the thermodynamic sense and in fact T_{DM} is simply meant to quantify the average velocity dispersion over the three spatial directions. Any completely spherically symmetric and relaxed DM configuration obeys the Jeans equation

$$\sigma_r^2 \left(\frac{d \ln \rho_{\text{DM}}}{d \ln r} + \frac{d \ln \sigma_r^2}{d \ln r} + 2\beta \right) + \frac{GM_{\text{tot}}(r)}{r} = 0, \quad (6)$$

where $\rho_{\text{DM}}(r)$ denotes the DM density profile (Binney & Tremaine 1987).

3. The temperature profile

Early studies of the X-ray emission from regular clusters were based on the assumption of an *isothermal* gas distribution, simply because the *Einstein* observatory and ROSAT were unable to determine the cluster temperature profiles. The observed X-ray emission is produced by thermal bremsstrahlung (Sarazin 1986), so for $T_g = \text{const.}$ it follows that $\rho_g(r)$ is proportional to the square root of the deprojected X-ray surface brightness. In such a situation, a good fit to the data was provided by the beta-model (Cavaliere & Fusco-Femiano 1976; Sarazin 1986)

$$\rho_g(r) = \frac{\rho_g(0)}{\left[1 + \left(\frac{r}{a_X} \right)^2 \right]^{3\beta_{\text{fit}}/2}}, \quad (7)$$

where $a_X < 0.5$ Mpc is the X-ray core radius. Note that β_{fit} has nothing to do with the DM velocity anisotropy. Typically, most of the emission comes from the region $r > 0.5$ Mpc, and so Eq. (7) can be approximated by the power-law

$$\rho_g(r) \simeq \rho_g(0) \left(\frac{r}{a_X} \right)^{-3\beta_{\text{fit}}}. \quad (8)$$

Now, by inserting Eq. (8) and $T_g = \text{const.}$ into Eq. (1), we find

$$M_{\text{tot}}(r) = \left(\frac{3\beta_{\text{fit}}\sigma_g^2}{G} \right) r, \quad (9)$$

where Eq. (2) has been used. As is well known, under the assumption of isotropic velocity distribution ($\beta = 0$), a mass profile of the form $M(r) \propto r$ describes a singular isothermal sphere (SIS) model

in which the velocity dispersion is everywhere constant (Binney & Tremaine 1987). Denoting by σ the one-dimensional velocity dispersion, we explicitly have $M(r) = (2\sigma^2/G)r$. Owing to the fact that the leading contribution to $M_{\text{tot}}(r)$ comes from DM, it follows that $M_{\text{tot}}(r) \simeq M_{\text{DM}}(r)$. As a consequence, Eq. (9) can be rewritten as

$$M_{\text{DM}}(r) \simeq \left(\frac{2\sigma_{\text{DM}}^2}{G} \right) r \quad (10)$$

and the comparison of Eqs. (9) and (10) entails in turn

$$\sigma_{\text{DM}}^2 \simeq 1.5 \beta_{\text{fit}} \sigma_g^2. \quad (11)$$

Observations performed with the *Einstein* observatory and ROSAT yield $0.5 < \beta_{\text{fit}} < 0.9$ with a median $\beta_{\text{fit}} \simeq 0.67$ (Bahcall & Lubin 1994). Thus, on average we get

$$\sigma_{\text{DM}}^2 \simeq \sigma_g^2, \quad (12)$$

which implies

$$T_{\text{DM}} \simeq T_g, \quad (13)$$

thanks to Eqs. (2) and (5).

Only with the advent of the ASCA and *Beppo-SAX* satellites did it become possible to measure the cluster temperature profiles, which turned out to be described by a polytropic gas distribution to first approximation. Higher-quality data are currently provided by *Chandra* and *XMM-Newton* satellites, which have shown that the gas temperature profiles possess a very simple and nearly universal behaviour (see Vikhlinin et al. (2006) for a thorough discussion). Basically, it increases rapidly from a small (possibly non-zero) value in the centre, to a maximum at a radius about $0.1 r_{180}$, and then declines slowly by a factor of $2 - 3$ at $(0.6 - 0.8) r_{180}$. Here, r_{180} is defined as the radius within which the mean total density is 180 times the critical density at the redshift of the cluster. The necessary X-ray background subtraction makes it very difficult to accurately measure the temperature further out.

As mentioned above, our main goal is the determination of the gas density profile $\rho_g(r)$ once a specific dark matter distribution $M_{\text{DM}}(r)$ is given. Supposing as before that $M_{\text{tot}}(r) \simeq M_{\text{DM}}(r)$, it is evident that $\rho_g(r)$ follows from Eq. (1) provided that $T_g(r)$ is specified. Previous studies (Makino

et al. 1997; Suto et al. 1998) accomplished this task by assuming

$$T_g(r) \simeq \frac{G\mu m_p M_{\text{DM}}(r)}{3k_B r}, \quad (14)$$

which was claimed to formalize the condition that the gas temperature is close to the virial temperature of the DM. However, the virial theorem is a global relation that characterizes a cluster as a whole – it just arises by integrating the Jeans equation over the system – and so it makes no sense physically to assume its local validity, as Eq. (14) would instead presuppose.

As a matter of fact, this stumbling block can be side-stepped in a remarkably simple fashion. Because of the equivalence principle, the velocity of a test particle in an external gravitational field is independent of the particle mass. This circumstance leads to the guess

$$T_{\text{DM}}(r) = \kappa T_g(r). \quad (15)$$

This relation was tested against numerical simulations (Host et al. 2009), which demonstrated its validity with $\kappa = 1$ to a very good approximation. These numerical simulations (Kay et al. 2007; Springel 2005; Valdarnini 2006) are reliable only on scales greater than $\sim 0.1 r_{2500}$, while the best X-ray observations are sensitive to a radius which is almost a factor 3 smaller. It is therefore possible that heating or cooling may shift κ away from unity in the very centre. Hence, outside that region $\kappa = 1$ is expected. Actually, a look back at Eq. (13) confirms the remarkable fact that $\kappa = 1$ holds regardless of the actual shape of the DM velocity anisotropy profile $\beta(r)$. As we shall see, starting from a specific underlying DM density profile $\rho_{\text{DM}}(r)$, one can evaluate $T_{\text{DM}}(r)$ and then get the gas temperature profile $T_g(r)$ uniquely.

Before closing this section, a remark is in order. Observations show that some clusters lack a central cooling flow. In such a situation, hydrostatic equilibrium is expected to hold all the way down to the centre. Actually, for typical central values of the electron number density $n_e \simeq 1 \text{cm}^{-3}$ and temperature $T \simeq 10^8 \text{K} \simeq 8.5 \text{keV}$ (Sarazin 1986), the scattering time turns out to be $t_{\text{scat}} \sim 10^2 \text{yr}$, which is much smaller than the corresponding gas cooling time $t_{\text{cool}} \sim 10^7 \text{yr}$, so that local hydrostatic equilibrium is indeed fulfilled outside a central spherical region of radius $\sim 1 \text{pc}$. Assuming

further that the gas temperature is roughly constant in the inner cluster region, the gas density profile cannot be cuspy as long as $M_{\text{DM}}(r) \propto r^a$ with $a > 1$ for $r \rightarrow 0$. This is at odds with blind extrapolations of fitting formulae for the temperature and density such as those used in Vikhlinin et al. (2006).

4. The density profile

We now proceed to the actual derivation of the gas density profile $\rho_g(r)$ from the properties of the dominating DM distribution.

As a preliminary step, we notice that Eqs. (1) and (6) can be trivially combined to yield

$$\begin{aligned} & \frac{k_B T_g}{\mu m_p} \left(\frac{d \ln \rho_g}{d \ln r} + \frac{d \ln T_g}{d \ln r} \right) \\ &= \sigma_r^2 \left(\frac{d \ln \rho_{\text{DM}}}{d \ln r} + \frac{d \ln \sigma_r^2}{d \ln r} + 2\beta \right). \end{aligned} \quad (16)$$

Owing to Eqs. (5) and (15) with $\kappa = 1$, straightforward manipulations permit to recast Eq. (16) into the form

$$\gamma_g = \frac{1}{1 - \frac{2}{3}\beta} \left(\gamma_{\text{DM}} + 2\beta + \frac{2}{3}\beta \frac{d \ln \sigma_r^2}{d \ln r} + \frac{2}{3} \frac{d\beta}{d \ln r} \right), \quad (17)$$

where we have defined the density slopes $\gamma_{\text{DM}}(r)$ of the DM and $\gamma_g(r)$ of the gas as

$$\gamma_X(r) \equiv \frac{d \ln \rho_X}{d \ln r}, \quad (18)$$

with X standing for either DM or g . We stress that Eq. (17) captures a crucial point of the present investigation: only the gas density slope appears on its left-hand side, whereas only quantities pertaining to the DM appear on its right-hand side. It should be appreciated that this result merely relies upon the equality of gas and DM temperatures and – unlike in previous studies (Cavaliere & Fusco-Femiano 1976; Makino et al. 1997; Suto et al. 1998) – no assumption is being made about the actual gas temperature structure (e.g. isothermal or polytropic).

Next, we use the fact that the DM anisotropy profile $\beta(r)$ turns out to be almost linearly related to the slope of the DM density profile $\gamma_{\text{DM}}(r)$. This result has been obtained from numerical simulations and holds with a scatter of about 0.05 (Hansen & Moore 2006; Hansen & Stadel 2006).

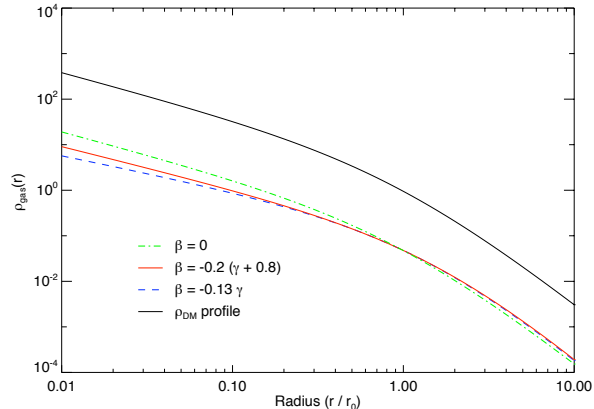


Fig. 1.— The derived gas density profile, assuming that $\rho_g/\rho_{\text{DM}} = 10\%$ at r_0 , which is the scale length of the NFW profile. The upper curve (black) is the DM density, and the 3 lower lines show gas profiles modelled with extreme variations in the possible DM velocity anisotropy (green dot-dashed is isotropic ($\beta = 0$), red solid is using $\beta = -0.2(\gamma + 0.8)$ (Hansen & Stadel 2006), and blue dashed is using $\beta = -0.13\gamma$ (Hansen 2008)).

It has recently been confirmed by high-resolution numerical simulations (Navarro et al. 2008) and moreover it has been derived analytically (Hansen 2008) (see also Zait et al. (2008); Wojtak et al. (2008); Salvador-Solé et al. (2007)).

Getting the gas density profile $\rho_g(r)$ now involves a few simple steps. Our only input is the DM density profile $\rho_{\text{DM}}(r)$, like e.g. an NFW profile. Thanks to Eq. (18), we rewrite the Jeans equation (6) as

$$r \frac{d\sigma_r^2}{dr} + \sigma_r^2 \left(\gamma_{\text{DM}}(r) + 2\beta(r) \right) + \frac{GM_{\text{tot}}(r)}{r} = 0, \quad (19)$$

whose solution is easily found to be

$$\sigma_r^2(r) = \frac{G}{B(r)} \int_r^\infty dr' \frac{B(r') M_{\text{tot}}(r')}{r'^2}, \quad (20)$$

with

$$B(r) \equiv \rho_{\text{DM}}(r) \exp \left\{ -2 \int_r^\infty dr' \frac{\beta(r')}{r'} \right\}. \quad (21)$$

Using the relation between $\beta(r)$ and $\gamma_{\text{DM}}(r)$, we finally obtain the gas density profile from Eqs. (17) and (18).

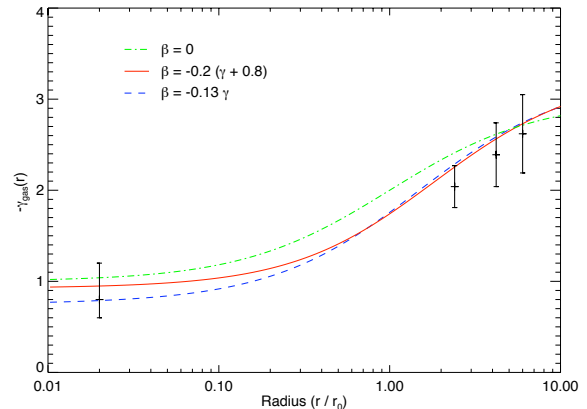


Fig. 2.— The derived slope of the gas density profile, assuming an NFW profile for the DM. Same notation as in Figure 1. The inner point is taken from Vikhlinin et al. (2006) and the three outer points are taken from Ettori & Balestra (2008).

In practice, such a procedure can be implemented iteratively. In first approximation, we assume that the gas mass contribution is negligible, so that we have $M_{\text{tot}}(r) = M_{\text{DM}}(r)$. In the next iterations, we include the gas mass in the calculation of $\sigma_r^2(r)$. Although the gas mass is taken into account perturbatively, any desired accuracy can be achieved by a sufficient number of iterations.

An example of the application of this strategy is shown in Figure 1, where the DM density is assumed to follow an NFW profile (black solid line). The three lower lines are the gas density profiles obtained with a range of different possible DM velocity anisotropy profiles. The details of the gas density profile are easier seen in the slope, which is shown in Figure 2. Note that for an inner DM slope of about 1 (in agreement with the observations (Voigt & Fabian 2006; Pointecouteau et al. 2005)) the inner *gas* slope should also be close to 1. This is in good agreement with the fits from Vikhlinin et al. (2006), which have an average of 0.8 for the extrapolated inner slope. Also the slopes found by Ettori & Balestra (2008) agrees with an NFW profile.

A widely used alternative to the NFW profile is the Sersic (or Einasto) profile, which generalizes the de Vaucouleurs profile traditionally used to fit the optical surface brightness of elliptical galaxies. It has been shown that the Sersic profile models

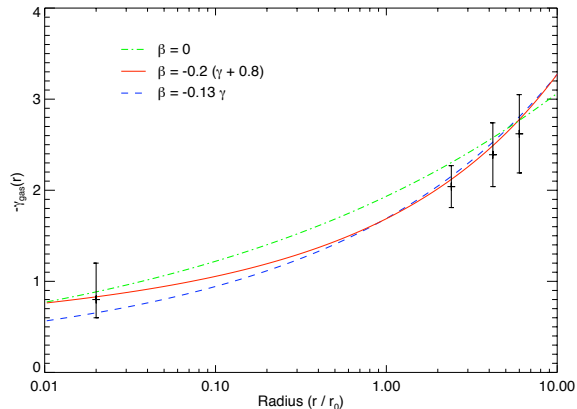


Fig. 3.— The slope of the gas density profile, assuming a Sersic profile with $n = 5$ for the DM. Same notation as in Figures 1 and 2.

the deprojected DM density at least as well as the NFW (Navarro et al. 2004; Merritt et al. 2006; Salvador-Solé et al. 2007). This profile contains 3 free parameters: two scaling constants for the density and the radius – ρ_0 and r_0 respectively – and one shape parameter n

$$\rho(r) = \rho_0 \exp \left[-b_n \left(\left(\frac{r}{r_0} \right)^{\frac{1}{n}} - 1 \right) \right]. \quad (22)$$

The constant b_n is a function of the index n and is tabulated e.g. by Mazure & Capelato (2002). The radial velocity dispersion σ_r derived from the Sersic profile has, like the NFW profile, the property of reaching its maximum near r_0 where the slope is $\gamma = 2$. In Figure 3 we present the gas density slope, assuming a Sersic profile for the underlying DM density. There is not sufficient statistical power in the data to discriminate between the underlying DM density and/or velocity anisotropy profiles from this analysis.

Both the NFW and the Sersic profile are consistent with observations because they have the appropriate slope in the inner and outer observed region. Since we cannot exclude one or the other by relying upon their shape, we choose the NFW model for the underlying DM in the rest of our treatment.

Since the gas density profile differs from the underlying DM density profile, there will also be a radial variation in the local and cumulative gas

fractions, which are defined as

$$\phi_g(r) = \frac{\rho_g(r)}{\rho_{\text{tot}}(r)} \quad (23)$$

and

$$f_g(r) = \frac{M_g(r)}{M_{\text{tot}}(r)}, \quad (24)$$

respectively. In order to test this in more detail, we used the 16 clusters analysed in Host et al. (2009), which is a selection of highly relaxed clusters at both low and intermediate redshifts (Kaasstra et al. 2004; Piffaretti et al. 2005; Morandi et al. 2007) observed with *XMM-Newton* and *Chandra*. Under the assumption of hydrostatic equilibrium, we find the local gas fraction exhibited in Figure 4. The local gas fraction clearly increases as a function of radius, which demonstrates that the DM velocity anisotropy cannot vanish (green dot-dashed line in Figure 4). The gas density fraction roughly increases as a power-law in radius and we have approximately $f_g(r) \sim r^{0.5}$. The solid (red) and dashed (blue) lines are for NFW DM profiles, with different radial DM velocity anisotropies. From Figure 4 there is a clear difference between the data and the predictions in the outer region, which may be due to an underestimation of the total mass due to breakdown of hydrostatic equilibrium (Piffaretti & Valdarnini 2008).

It is important to keep in mind that these profiles do not contain any free parameters. Every quantity is calculated from the dark matter distribution alone.

The agreement in the inner region is better and it should be kept in mind that different DM density and velocity anisotropy profiles give rise to different curves. It may therefore be possible to use the shape of $\phi_g(r)$ to recover these DM profiles in the future.

As a further step, we discuss some of the implications of our main result. Indeed, with a full description of the gas that is directly derived from the dark matter distribution, we can predict additional observable quantities besides the gas fraction described above.

One of these quantities is the entropy, which is often characterized by the adiabatic coefficient K_g of the gas

$$K_g = \frac{k_B T}{\mu m_p} \rho^{-2/3} = \sigma_g^2 \rho^{-2/3}. \quad (25)$$

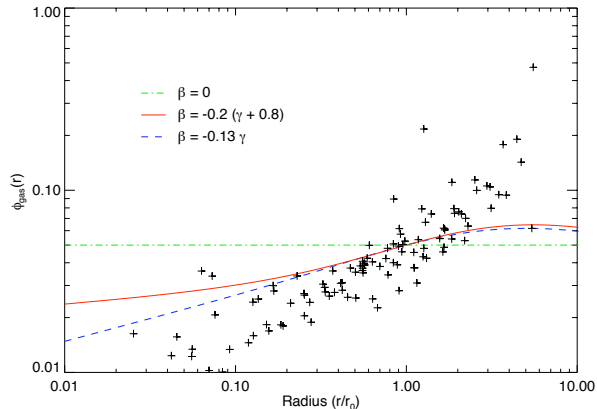


Fig. 4.— The observed ϕ_g from 16 relaxed galaxy clusters. We have scaled the gas mass fraction with free parameters, to make the radial variation more visible. There is a rough trend that the gas mass fraction increases as $r^{0.5}$, which is in clear disagreement with the assumption that the DM velocity anisotropy should vanish. The 3 curves all assume an NFW density profile, and different assumed connections between the DM slope and velocity anisotropy, as in Figure 1.

Our previous results entail that these profiles are almost perfect power laws regardless of the β profile. The slope changes slightly for the different β profiles (between 1.1 and 1.3). This theoretical prediction is in good agreement with the X-ray observations, which generally produce power-law entropy profiles (Piffaretti et al. 2005; Pratt, G. W. & Arnaud, M. 2005; Donahue et al. 2006).

Another quantity that we are able to predict is the gas X-ray emissivity ϵ . As a matter of fact, ϵ can be estimated either analytically – because $\epsilon \propto n^2 T^{1/2}$ – or by numerical codes like MeKaL (Mewe et al. 1985) in order to include the line emission contribution. The latter strategy is especially well suited for cooler clusters, because a substantial amount of their luminosity stems from emission lines. On the other hand, the luminosity of hotter clusters is dominated by the continuum emission. In either case, the surface brightness can be inferred from a given DM profile and this can in turn be compared with observations. In this way, it is possible to construct an algorithm that adjusts the proposed DM profile until the surface brightness best-fits observations and thereby sin-

gle out the optimal DM profile.

Whereas numerical simulations have demonstrated that the gas and dark matter temperatures are equal in large parts of a galaxy cluster, they cannot probe the very centre of the clusters. It is therefore possible that κ in Eq. (15) departs from unity as $r \rightarrow 0$ if there is significant cooling or heating. However, in our derivation of the gas density profile we have assumed $\kappa = 1$ everywhere.

It goes without saying that we can turn the argument around and use the observed gas profile to determine κ . Basically, we can insert Eq. (15) into Eq. (16) and solve for κ . Furthermore, since we are now interested in the central region where β is likely to be vanishingly small, we discard all terms involving β in the resulting equation. So, in place of Eq. (17) we presently get

$$\kappa = \frac{\gamma_g + d \ln \sigma_r^2 / d \ln r}{\gamma_{\text{DM}} + d \ln \sigma_r^2 / d \ln r}, \quad (26)$$

which in principle allows to measure κ directly from X-ray observations. Such measurement can be used or tested in future numerical simulations when the increased particle number will allow simulations to probe closer to the cluster centre.

5. Conclusions

We have shown that all properties of the hot X-ray emitting gas in galaxy clusters are completely determined by its underlying DM structure. Apart from the condition of hydrostatic equilibrium for the gas and the Jeans equation for the DM, our derivation rests upon two simple relations which have recently emerged from numerical simulations. One is the equality of the gas and DM temperatures. The other is an almost linear relationship between the DM velocity anisotropy profile and its density slope. For DM distributions described by the NFW or the Sersic profiles, the resulting gas density profile, the gas-to-total-mass ratio profile and the entropy profile are all in good agreement with X-ray observations. We feel that our result is conceptually relevant in itself. Moreover, it allows to predict the X-ray luminosity profile of a cluster in terms of its DM content alone. Therefore, a new strategy becomes available to constrain the DM morphology in galaxy clusters from X-ray observations (Frederiksen et al. 2009). This strategy may constrain morphology parameters better be-

cause of the tighter errors on surface brightness, but requires the structure to be very relaxed and thus cannot be used on every cluster. Our results can also be used as a practical tool for creating initial conditions for realistic cosmological structures to be used in numerical simulations. We plan to come back to the latter issues in great detail elsewhere.

Acknowledgements

It is a pleasure to thank Andrea Morandi and Rocco Piffaretti for letting us use their reduced X-ray observations. One of us (M. R.) thanks the Dipartimento di Fisica Nucleare e Teorica, Università di Pavia, for support. The Dark Cosmology Centre is funded by the Danish National Research Foundation.

REFERENCES

- Allen, S. W., Schmidt, R. W., Ebeling, H., Fabian, A. C., & van Speybroeck, L. 2004, *MNRAS*, 353, 457
- Bahcall, N. A., & Lubin L. M. 1994, *ApJ*, 426, 513
- Binney, J., & Tremaine, S. 1987, Princeton, NJ, Princeton University Press, 1987.
- Carlberg, R. G., et al. 1997, *ApJ*, 485, L13
- Cavaliere, A., & Fusco-Femiano, R. 1976, *A&A*, 49, 137
- Cole, S., & Lacey, C. 1996, *MNRAS*, 281, 716
- De Grandi, S., & Molendi, S. 2002, *ApJ*, 567, 163
- Diemand, J., Moore, B., & Stadel, J. 2004, *MNRAS*, 353, 624
- Donahue, M., Horner, D. J., Cavagnolo, K. W., & Voit, G. M. 2006, *ApJ*, 643, 730
- Ettori, S. & Balestra, I. *ArXiv e-prints*, 2008, arXiv:0811.3556 [astro-ph].
- Fabricant, D, Lecar, M. & Gorenstein, P. 1980, *ApJ*241, 552
- Frederiksen et al. 2009, in preparation
- Merritt, D., Graham, A. W., Moore, B., Diemand, J., & Terzić, B. 2006, *AJ*, 132, 2685
- Hansen S. H., & Moore B 2006, *New Astron.*, 11, 333
- Hansen, S. H., & Stadel, J. 2006, *Journal of Cosmology and Astro-Particle Physics*, 5, 14
- Hansen, S. H., & Piffaretti, R. 2007, *A&A*, 476, L37
- Hansen, S. H. 2008, arXiv:0812.1048
- Host, O., Hansen, S. H., Piffaretti, R., Morandi, A., Ettori, S., Kay, S. T., & Valdarnini, R. 2009, *Astrophys. J.* 690, 358
- Kaastra, J. S., et al. 2004, *A&A*, 413, 415
- Kay, S. T., da Silva, A. C., Aghanim, N., Blanchard, A., Liddle, A. R., Puget, J.-L., Sadat, R., & Thomas, P. A. 2007, *MNRAS*, 377, 317
- Makino, N., Sasaki, S. & Suto, Y. 1998, *ApJ*, 497, 555
- Mazure, A. & Capelato, H. V. *A&A*, 2002, 383, 384-389
- Mewe, R.; Gronenschild, E. H. B. M. & van den Oord, G. H. J. *A&AS*, 1985, 62, 197-254
- Moore, B., Governato, F., Quinn, T., Stadel, J. & Lake G. 1998, *ApJ*, 499, 5
- Morandi, A., Ettori, S., & Moscardini, L. 2007, *MNRAS*, 379, 518
- Navarro, J. F., Frenk, C. S., & White, S. D. M. 1996, *ApJ*, 462, 563
- Navarro, J. F., et al. 2004, *MNRAS*, 349, 1039
- Navarro, J. F. et al. 2008, arXiv:0810.1522
- Piffaretti, R., Jetzer, P., Kaastra, J. S. & Tamura, T. *A&A*, 2005, 433, 101-111
- Piffaretti, R. & Valdarnini, R. 2008, arXiv:0808.1111
- Pratt, G. W. & Arnaud, M. *A&A*, 2005, 429, 791-806
- Pointecouteau, E., Arnaud, M., & Pratt, G. W. 2005, *Astron. & Astrophys*, 435, 1
- Salvador-Solé, E., Manrique, A., González-Casado, G., & Hansen, S. H. 2007, *ApJ*, 666, 181

- Sarazin, C. L. 1986, *Reviews of Modern Physics*, 58, 1
- Springel, V. 2005, *MNRAS*, 364, 1105
- Stadel, J. et al. 2008, arXiv:0808.2981
- Suto, Y., Sasaki, S., & Makino, N. 1998, *ApJ*, 509, 544
- Valdarnini, R. 2006, *New Astron.* 12, 71
- Vikhlinin, A., Markevitch, M., Murray, S. S., Jones, C., Forman, W., & Van Speybroeck, L. 2005, *ApJ*, 628, 655
- Vikhlinin, A., Kravtsov, A., Forman, W., Jones, C., Markevitch, M., Murray, S. S., & Van Speybroeck, L. 2006, *Astrophys. J.* 640, 691
- Voigt, L. M., & Fabian, A. C. 2006, *MNRAS*, 368, 518
- Wojtak, R., Lokas, E. L., Mamon, G. A., Gottlöber, S., Klypin, A., & Hoffman, Y. 2008, *MNRAS*, 388, 815
- Zait, A., Hoffman, Y., & Shlosman, I. 2008, *ApJ*, 682, 835

Appendix C

Source Code

C.1 kappa1.pro

This is the driver-program for producing all the plot in chapter 3. The program calculates all the quantities from a dark matter density.

```
pro kappa1

;--- Print output to file? ---
PRN=0
if (PRN eq 1) then begin
    set_plot, 'PS'
    device, filename='kappa1.ps'
endif

;--- Define arrays ---
Num = 1000
M = dblarr(Num)
Mgas = dblarr(Num)
sigma2 = dblarr(Num)
flip = -indgen(Num) + Num-1

; --- Generate legends ---
d = !d.name
set_plot, 'PS'
p = !p.font
```

```

!p.font = 0
  legendtext = textoidl(['\beta = -0.13 \gamma', '\beta = -0.2 (\gamma + 0.8)',
  legendx = textoidl('Radius (r / r_0)')
  legendgamma = textoidl('-\gamma(r)')
  legendbeta = textoidl('\beta(r)')
  legendsigma2 = textoidl('\sigma^2_r(r)')
  legendgasslope = textoidl('-\gamma_{gas}(r)')
  legendrhogas = textoidl('\rho_{gas}(r)')
  legendrhodm = textoidl('\rho_{DM} profile')
  legendMgas = textoidl('M_{gas}(r)')
  legendMdm = textoidl('M_{DM}')
  legendfgas = textoidl('f_{gas}(r)')
  legendfgas2 = textoidl('\phi(r)')
  legendentropy = textoidl('K_{gas}(r)')
  legendentropydm = textoidl('K_{dm}(r)')
!p.font = p
set_plot, d

;--- Initialize ---
p = .05d ; gas fraction
xmin = -2.
xmax = 2.
x = 10^( dindgen(Num)/Num * ( xmax - xmin ) + xmin )

; ++++++
; +++++ Density-profile +++++
; ++++++

NFWprofile = 1
if (NFWprofile eq 1) then begin
  ; -- Double-powerlaw --
  Inner = 1
  outer = 3
  bend = 1.
  rho = 1 / ( x^Inner * ( 1 + x^Bend )^((Outer - Inner)/Bend) )
  prefix = '_nfw'
endif else begin
  ; -- Sersic-profil

```

```

n = 5.
dn = 9.6687 ; for n=5
rho = exp( -dn * ( x^(1./n) - 1. ) )
rho = rho/rho[Num/2]
prefix = '_sersic'
endelse

; ++++++
; ++++++ End of Density-profile ++++++
; ++++++

; calc M from rho
M = 4*!pi*intloglog( x, x^2 * rho )

; --- calc rho from M ---
rho = dydx(x,M)/(4*!pi*x^2)
rho = rho/rho[Num/2]

; --- calc gamma from rho ---
gamma = dlndlnx( x, rho )

; --- calc beta ---
beta1 = -.13 * gamma
Beta2 = .2 * ( -gamma - .8 )
beta3 = 0 * gamma

epsplot, x, beta1, beta2, beta3, /xlog, $
  yrange=[-.5,1], $
  xrange=[0.01,10], $
  color=[3, 1, 2], $
  linestyle=[2, 0, 3], $
  thick=3, $
  xtitle=legendx, $
  ytitle=legendbeta, $
  xylegend=[0.25, 0.75], $
  legend=legendtext, $
  file='beta'+prefix+'.eps'

```

```

epsplot, -gamma, beta1, beta2, beta3, $
  yrange=[-.5,1], $
  xrange=[1,3], $
  color=[3, 1, 2], $
  linestyle=[2, 0, 3], $
  thick=3, $
  xtitle=legendgamma, $
  ytitle=legendbeta, $
  xylegend=[0.25, 0.75], $
  legend=legendtext, $
  file='gammabeta'+prefix+'.eps'

; --- calc sigma from rho, M and beta ---
r = intloglog2(x,gamma + 2*beta1)          ; rho-tilde
y = M*r/x^2                               ; the integrand
sigma1 = intloglog( x[flip], -y[flip] )
sigma1 = sigma1[flip]
sigma1 = sigma1/r
sigma1 = sigma1/sigma1[Num/2]
r = intloglog2(x,gamma + 2*beta2)
y = M*r/x^2
sigma2 = intloglog( x[flip], -y[flip] )
sigma2 = sigma2[flip]
sigma2 = sigma2/r
sigma2 = sigma2/sigma2[Num/2]
r = intloglog2(x,gamma + 2*beta3)
y = M*r/x^2
sigma3 = intloglog( x[flip], -y[flip] )
sigma3 = sigma3[flip]
sigma3 = sigma3/r
sigma3 = sigma3/sigma3[Num/2]
epsplot, x, sigma1, sigma2, sigma3, $
  /xlog, /ylog, $
  xrange=[0.01,10], $
  color=[3, 1, 2], $
  linestyle=[2, 0, 3], $
  thick=3, $
  xtitle=legendx, $

```

```

ytitle=legendsigma2, $
xylegend=[0.25, 0.75], $
legend=legendtext, $
file='sigma2'+prefix+'.eps'

; --- calc derivativ of sigma ---
logdydx1 = dlndlnx( x, sigma1 )
logdydx2 = dlndlnx( x, sigma2 )
logdydx3 = dlndlnx( x, sigma3 )

; --- calc d(beta)/dlnr ---
dbdr1 = x*dydx(x, beta1)
dbdr2 = x*dydx(x, beta2)
dbdr3 = x*dydx(x, beta3)

; --- The Gas equation ---
gasslope1 = ( 1.5*gamma + 3*beta1 + beta1*logdydx1 + dbdr1 ) / ( 1.5 - beta1 )
gasslope2 = ( 1.5*gamma + 3*beta2 + beta2*logdydx2 + dbdr2 ) / ( 1.5 - beta2 )
gasslope3 = ( 1.5*gamma + 3*beta3 + beta3*logdydx3 + dbdr3 ) / ( 1.5 - beta3 )

; --- data point from Ettori&Balestra and Vikhlinin ---
err = [[0.4*6, 0.7*6, 1.0*6, 0.02], $
       [ 2.04, 2.39, 2.62, 0.8], $
       [ 0.23, 0.35, 0.43, 0.2], $
       [ 0.23, 0.35, 0.43, 0.4] ]

epsplot, x, -gasslope1, -gasslope2, -gasslope3, $
/xlog, $
color=[3, 1, 2], $
linestyle=[2, 0, 3], $
th = 3, $
xrange=[0.01,10], $
yrange=[0,4], $
xtitle=legendx, $
ytitle= legendgasslope, $
points = err, $
xylegend=[0.25, 0.75], $
legend=legendtext, $

```

```

file='gasslope'+prefix+'.eps'

; --- calc Mgas from gas-slope ---
rhogas1 = intloglog2(x, gasslope1)
rhogas2 = intloglog2(x, gasslope2)
rhogas3 = intloglog2(x, gasslope3)

epsplot, x, rho, (p*rhogas1), (p*rhogas2), (p*rhogas3), $
  /xlog, /ylog, $
  xrange=[0.01,10], $
  yrange=[1e-4, 1e3], $
  color=[0, 3, 1, 2], $
  linestyle=[0, 2, 0, 3], $
  th = [1, 3, 3, 3], $
  xtitle=legendx, $
  ytitle=legendrhogas, $
  xylegend=[0.25, 0.25], $
  legend=[legendrhomd, legendtext], $
  file='rhogas'+prefix+'.eps'

; --- Rescaling ---
Mgas1 = intloglog(x, rhogas1*x^2)
Mgas1 = Mgas1 / Mgas1[Num/2] * M[Num/2]
Mgas2 = intloglog(x, rhogas2*x^2)
Mgas2 = Mgas2 / Mgas2[Num/2] * M[Num/2]
Mgas3 = intloglog(x, rhogas3*x^2)
Mgas3 = Mgas3 / Mgas3[Num/2] * M[Num/2]
epsplot, x, (p*Mgas1), (p*Mgas2), (p*Mgas3), M, $
  /xlog, /ylog, $
  xrange=[0.01,10], $
  color=[3, 1, 2,0], $
  linestyle=[2, 0, 3, 0], $
  th = [3,3,3,1], $
  xtitle=legendx, $
  ytitle=legendMgas, $
  legend=[legendtext, legendMdm], $
  xylegend=[0.25, 0.75], $
  file='Mgas'+prefix+'.eps'

```

```

fgas1 = p*Mgas1/M
fgas2 = p*Mgas2/M
fgas3 = p*Mgas3/M
epsplot, x, fgas1, fgas2, fgas3, $
  /xlog, $
  color=[3, 1, 2], $
  linestyle=[2, 0, 3], $
  thick = 3, $
  xrange=[0.01,10], $
  yrange=[0, 0.15], $
  xtitle=legendx, $
  ytitle=legendfgas, $
  xylegend=[0.25, 0.75], $
  legend=legendtext, $
  file='fgas'+prefix+'.eps'

```

```

fgas1 = p*rhogas1/rho
fgas2 = p*rhogas2/rho
fgas3 = p*rhogas3/rho
epsplot, x, fgas1, fgas2, fgas3, $
  /xlog, $
  color=[3, 1, 2], $
  linestyle=[2, 0, 3], $
  thick = 3, $
  xrange=[0.01,10], $
  yrange=[0, 0.15], $
  xtitle=legendx, $
  ytitle=legendfgas2, $
  xylegend=[0.25, 0.75], $
  legend=legendtext, $
  file='fgas2'+prefix+'.eps'

```

```

epsplot, x, $
  (sigma1/rhogas1^(2./3.)), $
  (sigma2/rhogas2^(2./3.)), $
  (sigma3/rhogas3^(2./3.)), $
  /xlog, /ylog, $

```

```

xrange=[0.01,10], $
yrange=[1e-4,1e4], $
color=[3, 1, 2], $
linestyle=[2, 0, 3], $
thick = 3, $
xtitle=legendx, $
ytitle=legendentropy, $
file='entropy_gas'+prefix+'.eps'
; Label Hack:
; xyouts, 0.70,0.50, 'NFW', /normal, charthick=2
; xyouts, 0.55,0.65, 'Sersic', /normal, charthick=2

epsplot, x, (sigma1/rho^(2./3)), (sigma2/rho^(2./3)), (sigma3/rho^(2./3)), $
/xlog, /ylog, $
xrange=[0.01,10], $
color=[3, 1, 2], $
linestyle=[2, 0, 3], $
thick = 3, $
xtitle=legendx, $
ytitle=legendentropydm, $
ytickformat='("K", e5)', $
xylegend=[0.25, 0.25], $
legend=legendtext, $
file='entropy_dm'+prefix+'.eps'

; --- Close output file if necessary ---
if (PRN eq 1) then begin
    device, /close
    set_plot, 'X'
endif

end

```

C.2 intloglog.pro

```
;
; Returns the integral of y from x0 to x
; The relative error goes like 1/N^2
;
function intloglog, x, y

    Num = min( [ n_elements(x), n_elements(y) ] )
    if (Num lt 10) then begin
        Print, 'INTLOGLOG: Not enough data'
        return, !values.f_NaN
    endif

    ret = dblarr(Num)

    ; Initial guess
    a = alog(y[4]/y[2])/alog(x[4]/x[2])
    ret[0] = x[0] * y[0] / (a + 1)

    ; --- Trapez-methoden ---
    for i = 1, Num-1 do $
        ret[i] = ret[i-1] + .5d * ( y[i] + y[i-1] ) * ( x[i] - x[i-1] )

    return, ret

end
```

C.3 intloglog2.pro

```
;
; solves the equation  $d\ln(f)/d\ln x = y$ 
;  $f = f(x)$  and  $y = y(x)$ 
; returning f
;
function intloglog2, x, y

    Num = min( [ n_elements(x), n_elements(y) ] )
    if (Num lt 2) then begin
        Print, 'INTLOGLOG2: Not enough data points'
        return, !values.f_NaN
    endif

    Ret = dblarr(Num)

    Ret[0]=1
    Ret[1]=Ret[0]*(x[1]/x[0])^y[0]
    for i = 2, Num-1 do $
        Ret[i]=Ret[i-2]*(x[i]/x[i-2])^y[i-1]

    Ret = Ret/Ret[Num/2]

    return, Ret
end
```

C.4 dydx.pro

```
;
; This function returns the slope of y
; (the relative error goes like 1/N^2 )
;
; ret = d(y) / d(x)
;
function dydx, x, y

Num = min( [ n_elements(x), n_elements(y) ] )
if (Num lt 2) then begin
Print, 'Not enough data to calc derivative'
return, !values.f_NaN
endif

Ret = dblarr(Num)

for i = 1, Num-2 do $
ret[i] = (y[i+1]-y[i-1])/(x[i+1]-x[i-1])
ret[0] = ret[1]-(x[1]-x[0])/(x[2]-x[1])*(ret[2]-ret[1])
ret[Num-1] = ret[Num-2]-(x[Num-2]-x[Num-1])/(x[Num-3]-x[Num-2])*(ret[Num-3]-ret[Num-2])

return, ret

end
```

C.5 dlnydlnx.pro

```
;
; This function returns the log-slope of y
; (the relative error goes like 1/N^2 )
;
; ret = dln(y) / dln(x)
;
function dlnydlnx, x, y

    Num = min( [ n_elements(x), n_elements(y) ] )
    if (Num lt 2) then begin
        Print, 'Not enough data to calc derivative'
        return, !values.f_NaN
    endif

    Ret = dblarr(Num)

    for i = 1, Num-2 do $
        ret[i] = alog(y[i+1]/y[i-1])/alog(x[i+1]/x[i-1])
    ret[0] = ret[1]*(ret[1]/ret[2])^(alog(x[1]/x[0])/alog(x[2]/x[1]))
    ret[Num-1] = ret[Num-2]*(ret[Num-2]/ret[Num-3])^(alog(x[Num-2]/x[Num-1])/alog(x[Num-1]/x[Num-2]))

    return, ret

end
```

Bibliography

- [1] J. Binney and S. Tremaine. *Galactic Dynamics: Second Edition*. Galactic Dynamics: Second Edition, by James Binney and Scott Tremaine. ISBN 978-0-691-13026-2 (HB). Published by Princeton University Press, Princeton, NJ USA, 2008., 2008.
- [2] A. Cavaliere and R. Fusco-Femiano. The Distribution of Hot Gas in Clusters of Galaxies. *Astronomy and Astrophysics*, 70:677–+, November 1978.
- [3] A. Cavaliere, A. Lapi, and R. Fusco-Femiano. Galaxy Clusters, a Novel Look at Diffuse Baryons Withstanding Dark Matter Gravity. *ArXiv e-prints*, March 2009.
- [4] J. Christensen-Dalsgaard. Stellar structure and evolution. Lecture Notes, Institut of Physics and Astronomy, University of Aarhus, January 2006.
- [5] J. M. Comerford and P. Natarajan. The observed concentration-mass relation for galaxy clusters. *Monthly Notices of the Royal Astronomical Society*, 379:190–200, July 2007.
- [6] W. Dehnen and D. E. McLaughlin. Dynamical insight into dark matter haloes. *Monthly Notices of the Royal Astronomical Society*, 363:1057–1068, November 2005.
- [7] S. Ettori and I. Balestra. The outer regions of galaxy clusters: Chandra constraints on the X-ray surface brightness. *ArXiv e-prints*, November 2008.
- [8] A. W. Graham, D. Merritt, B. Moore, J. Diemand, and B. Terzić. Empirical Models for Dark Matter Halos. III. The Kormendy Relation and

- the $\log\rho_e - \log R_e$ Relation. *Astronomical Journal*, 132:2711–2716, December 2006.
- [9] S. H. Hansen. Might we eventually understand the origin of the dark matter velocity anisotropy? *ArXiv e-prints*, December 2008.
- [10] S. H. Hansen and B. Moore. A universal density slope Velocity anisotropy relation for relaxed structures. *New Astronomy*, 11:333–338, March 2006.
- [11] S. H. Hansen, B. Moore, and J. Stadel. A universal density slope - velocity anisotropy relation. *ArXiv Astrophysics e-prints*, September 2005.
- [12] S. H. Hansen and J. Stadel. The velocity anisotropy — density slope relation. *Journal of Cosmology and Astro-Particle Physics*, 5:14–+, May 2006.
- [13] L. Hernquist. An analytical model for spherical galaxies and bulges. *Astrophysical Journal*, 356:359–364, June 1990.
- [14] O. Host, S. H. Hansen, R. Piffaretti, A. Morandi, S. Ettori, S. T. Kay, and R. Valdarnini. Measurement of the dark matter velocity anisotropy in galaxy clusters. *ArXiv e-prints*, 808, August 2008.
- [15] Joel Johansson. Dynamics of galaxy clusters. Master’s thesis, Dark Cosmology Centre, Niels Bohr Institute, University of Copenhagen, Denmark & The Royal Institute of Technology, Sweden, 2009.
- [16] J. T. Kleyna, M. I. Wilkinson, N. W. Evans, and G. Gilmore. First Clear Signature of an Extended Dark Matter Halo in the Draco Dwarf Spheroidal. *Astrophysical Journal Letters*, 563:L115–L118, December 2001.
- [17] R. A. Knop, G. Aldering, R. Amanullah, P. Astier, G. Blanc, M. S. Burns, A. Conley, S. E. Deustua, M. Doi, R. Ellis, S. Fabbro, G. Folatelli, A. S. Fruchter, G. Garavini, S. Garmond, K. Garton, R. Gibbons, G. Goldhaber, A. Goobar, D. E. Groom, D. Hardin, I. Hook, D. A. Howell, A. G. Kim, B. C. Lee, C. Lidman, J. Mendez, S. Nobili, P. E. Nugent, R. Pain, N. Panagia, C. R. Pennypacker, S. Perlmutter, R. Quimby, J. Raux, N. Regnault, P. Ruiz-Lapuente, G. Sainton,

- B. Schaefer, K. Schahmaneche, E. Smith, A. L. Spadafora, V. Stanishev, M. Sullivan, N. A. Walton, L. Wang, W. M. Wood-Vasey, and N. Yasuda. New Constraints on Ω_M , Ω_Λ , and w from an Independent Set of 11 High-Redshift Supernovae Observed with the Hubble Space Telescope. *Astrophysical Journal*, 598:102–137, November 2003.
- [18] L. D. Landau and E. M. Lifshitz. *Fluid Mechanics*. Pergamon Press, 1987.
- [19] M. Limousin, J. Richard, E. Jullo, J.-P. Kneib, B. Fort, G. Soucail, Á. Elíasdóttir, P. Natarajan, R. S. Ellis, I. Smail, O. Czoske, G. P. Smith, P. Hudelot, S. Bardeau, H. Ebeling, E. Egami, and K. K. Knudsen. Combining Strong and Weak Gravitational Lensing in Abell 1689. *Astrophysical Journal*, 668:643–666, October 2007.
- [20] D. Merritt, A. W. Graham, B. Moore, J. Diemand, and B. Terzić. Empirical Models for Dark Matter Halos. I. Nonparametric Construction of Density Profiles and Comparison with Parametric Models. *Astronomical Journal*, 132:2685–2700, December 2006.
- [21] R. Mewe, E. H. B. M. Gronenschild, and G. H. J. van den Oord. Calculated X-radiation from optically thin plasmas. V. *Astronomy and Astrophysics Supplement Series*, 62:197–254, November 1985.
- [22] J. F. Navarro, C. S. Frenk, and S. D. M. White. The Structure of Cold Dark Matter Halos. *Astrophysical Journal*, 462:563–+, May 1996.
- [23] J. F. Navarro, E. Hayashi, C. Power, A. R. Jenkins, C. S. Frenk, S. D. M. White, V. Springel, J. Stadel, and T. R. Quinn. The inner structure of Λ CDM haloes - III. Universality and asymptotic slopes. *Monthly Notices of the Royal Astronomical Society*, 349:1039–1051, April 2004.
- [24] R. Piffaretti and R. Valdarnini. Total mass biases in X-ray galaxy clusters. *Astronomy and Astrophysics*, 491:71–87, November 2008.
- [25] S. Riemer-Sørensen, D. Paraficz, D. D. M. Ferreira, K. Pedersen, M. Limousin, and H. Dahle. Resolving the Discrepancy Between Lensing and X-Ray Mass Estimates of the Complex Galaxy Cluster Abell 1689. *Astrophysical Journal*, 693:1570–1578, March 2009.

- [26] C. L. Sarazin. X-ray emission from clusters of galaxies. *Reviews of Modern Physics*, 58:1–115, January 1986.
- [27] K. B. Schmidt, S. H. Hansen, and A. V. Macciò. Alas, the Dark Matter Structures Were Not That Trivial. *Astrophysical Journal Letters*, 689:L33–L36, December 2008.
- [28] Kasper Borello Schmidt. Towards understanding dark matter structures. Master’s thesis, Dark Cosmologist Centre, Niels Bohr Institute, University of Copenhagen, Denmark, June 2008.
- [29] A. Vikhlinin, A. Kravtsov, W. Forman, C. Jones, M. Markevitch, S. S. Murray, and L. Van Speybroeck. Chandra Sample of Nearby Relaxed Galaxy Clusters: Mass, Gas Fraction, and Mass-Temperature Relation. *Astrophysical Journal*, 640:691–709, April 2006.
- [30] M. I. Wilkinson, J. T. Kleyna, N. W. Evans, G. F. Gilmore, M. J. Irwin, and E. K. Grebel. Kinematically Cold Populations at Large Radii in the Draco and Ursa Minor Dwarf Spheroidal Galaxies. *Astrophysical Journal Letters*, 611:L21–L24, August 2004.
- [31] H. Zhao. Analytical dynamical models for double power-law galactic nuclei. *Monthly Notices of the Royal Astronomical Society*, 287:525–537, May 1997.
- [32] F. Zwicky. Die Rotverschiebung von extragalaktischen Nebeln. *Helvetica Physica Acta*, 6:110–127, 1933.

Index

- A1689, *see* Abell 1689
- Abell 1689, 31
- Age of the Universe, 7
- Beta factor, The, 43
- CBE, 17
- Closed Universe, 7
- CMB, 7
- Collisionless Boltzmann equation, 17
- Conservation of mass, 13, 17
- Cosmic Microwave Background, *see* CMB
- Cosmological constant, The, 8
- Einstein, Albert, 6
- Epicyle, 5
- Euler equation, 13
- Flat Universe, 7
- Flux, 45
- Galileo, 5
- $\gamma \sim \beta$ relation, *see* Hansen-Moore relation
- Gas equation, The, 25, 41, 43
- Geocentric, 5
- Geodesics, 7
- Hansen-Moore relation, 49
- Hipparchus, 4
- Hubble, Edwin, 7
- Hydrostatic equilibrium, 14, 32
- ICM, 11
- ICP, *see* ICM
- Inter cluster plasma, *see* Inter cluster medium
- Intra cluster medium, 11
- Kepler, Johannes, 6
- Magnitude scale, 5
- Mass formula, 14
- Material derivative, 13
- MeKaL model, The, 33
- Microwave background Cosmic, *see* CMB
- Newton, Sir Isaac, 6
- Open Universe, 7
- Penzias & Wilson, 7
- Penzias, Arno, 7
- Phase-space, 15
- Ptolemaic world view, 5
- Ptolemy, 5
- Relativity theory
 - General, 6
 - Special, 6
- Sarazin, 25
- Substantial derivative, 13
- Surface Brightness

Definition, 43

Temperature

Dark Matter, 42

Tycho Brahe, 5

Wilson, Robert, 7

Xspec, 44

Flux, 45